*J. Indian Inst. Sci.*, Mar.–Apr. 2001, **81**, 181–212.


# IISc THESES ABSTRACTS

Thesis Abstract (Ph. D.)

**Studies of moisture-induced crosslinking in some novel vinyl ether–maleic anhydride copolymers and terpolymers and synthesis and characterization of hyperbranched polyketals** by B. Rema
Research supervisor: Prof. S. Ramakrishnan
Department: Inorganic and Physical Chemistry

## 1. Introduction

The present work deals with investigations on two distinct research areas, namely, (a) Synthesis and moisture-curing properties of novel vinyl ether–maleic anhydride copolymers and (b) Synthesis and properties of hyperbranched polyketals.

## 2a. Synthesis and moisture-curing properties of novel vinyl ether–maleic anhydride copolymers

Vinyl ethers can be copolymerized with electron-deficient olefins such as maleic anhydride, $\alpha$-chloro acrylonitrile, alkyl maleimides, etc. to give essentially alternating copolymers.[1] A wide variety of vinyl ethers have been copolymerized with maleic anhydride, with the motivation in most cases being the understanding of the underlying mechanism for the formation of such alternating copolymers. In some cases, however, the reactive anhydride functionality in the alternating copolymer backbone has been used to tether specific functional units, such as mesogens.[2] The present work deals with the synthesis of a novel vinyl either, 2,2-dimethyl-4-vinyloxymethyl-1,3-dioxolane (DMVMD) that has a dimethyl ketal protected vicinal diol functionality, from readily available starting materials, such as glycerol, acetone and acetylene. Copolymerisation of DMVMD with maleic anhydride (MAH) in various molar ratios was carried out using a free radical initiator. The composition of the copolymer was established by conductometric titration and was found to be 1:1 irrespective of the monomer feed composition thus establishing its alternating nature. The copolymer formed clear free-standing films upon solvent casting which became insoluble upon prolonged exposure to ambient atmosphere. The insolubility is ascribed to moisture-induced crosslinking. A plausible mechanism for the crosslinking involves the hydrolysis of some of the anhydride groups, followed by acid-catalyzed deketalization, and then by the reaction of the alcoholic groups, thus generated, with the residual anhydride to give ester crosslinks. This hypothesis was confirmed both by model reactions and *in situ* FT-IR studies. The first step in the crosslinking process is perceived to be the diffusion of water into the polymer film. The modulation of this diffusion process, should in principle permit the finetuning of the crosslinking rates. To this end, we carried out the terpolymerization studies wherein an additional hydrophobic [octyl vinyl ether (OVE)]/hydro-

philic [triethylene glycol monomethyl ether vinyl ether (TEGMVE)] vinylether is used as a comonomer. Two series of terpolymers with a systematic incorporation of hydrophilic (triethylene glycol monomethyl ether vinyl ether; TEGMVE) and hydrophobic (octyl vinyl ether, OVE) monomers, viz. TEGMVE/DMVMD/MAH and OVE/DMVMD/MAH were prepared. FT-IR spectroscopic studies demonstrate that by systematic incorporation of hydrophobic/hydrophilic comonomers, the water penetration and thus the crosslinking rate of the polymers can be controlled in a predictable fashion, viz. increase in hydrophilicity of the polymers, by increased incorporation of TEGMVE, increases the crosslinking rate, while increase in the hydrophobicity, by increased incorporation of OVE, retards it. The vinyl ether terpolymer study presented demonstrates that it is possible to 'custom design' polymers which undergo moisture-induced crosslinking at a predetermined rate. Such polymers are likely to have potential applications in coating technology.[3,4]

## 2b. Synthesis and properties of hyperbranched polyketals

The synthesis and characterization of dendrimers and hyperbranched polymers have attracted considerable attention recently. A dendritic macromolecule refers to any molecule prepared via an iterative methodology, where two or more sequential iterations are used to generate highly branched structures, wherein every repeat unit gives rise to one or more branches. The term dendritic molecule (or multiarmed[5] or cascade molecule[6]) can include single-tier polyfunctional structures as well as multigenerational architectures. The one-step synthesis of hyperbranched macromolecules utilizes an $AB_x$-type monomer (where A and B are functional groups, that react only with each other and not with itself) which undergoes a self-condensation polymerization.[7,8] The present work describes the synthesis of novel hyperbranched polyketals poly[2-(4-acetyl phenyl) ethylalcohol dimethyl ketal] (PPA) based on 4-acetyl phenyl ethylalcohol and poly(4-acetylphenyloxy ethylalcohol dimethyl ketal) (PPO) based on 4-acetyl phenyloxy ethyl alcohol by a *trans*-ketalization reaction of their corresponding dimethyl ketals ($AB_2$ monomers). The acid-catalyzed degradation of the polymers to their corresponding monomer precursors was followed by $^1$H NMR spectroscopy. The polymer PPO undergoes slower hydrolysis. It has phenyloxy units that are mesomerically capable of stabilizing carbocations better than the alkyl phenyl units present in polymer PPA. Since the hydrolysis process involves the generation of carbocationic intermediates one would expect from electronic considerations alone that the phenyloxy polymer PPO will undergo quicker hydrolysis. This is however not the case in the present system. One possible reason could be the difference in molecular weights between the two polymer samples; the former (PPO) having higher molecular weight undergoes slower degradation.

Tomalia and coworkers have studied the protonation of amine-terminated poly(amidoamines) dendrimers and found that the primary amines at the surface were more basic than the interior tertiary amines.[9] This has been ascribed to the fact that the interior tertiary amines of the dendrimers are not easily accessible to the protons in the solvent. From this observation one would expect that the higher molecular weight hyperbranched polyketal with larger number of interior ketal links (which are not readily accessible) would undergo slower hydrolysis. Thus, it appears that the difference in the molecular weight predominates the electronic effect in these systems. These polymers have potential biomedical[10] and environmental applications.[11]

This novel *trans*-ketalization methodology was further exploited to synthesize novel liquid crystalline hyperbranched polyketals, two series of polymers, viz. (a) poly[4-{4-(ω-hydroxy alkyloxy)phenyl}acetophenone dimethyl ketal] (PBPA(*n*)) based on 4-(4-(ω-hydroxy [alkyloxy)phenyl) acetophenones and (b) poly[4-{4-(ω-hydroxy olegoethylenoxy)phenyl} acetophenones dimethyl ketal] PBPOE(*n*) based on 4-(4-(ω-hydroxy olegoethylenoxy)phenyl) acetophenones were prepared by *trans*-ketalization of their corresponding dimethyl ketals ($AB_2$ monomers). The film-forming nature of the polymers indicates that they are of reasonably high molecular weight. The thermal properties of the monomer precursors and the polymers were studied by DSC in conjunction with polarized light microscopy. The nature of the liquid crystalline phase exhibited was probed by X-ray diffraction and polarized light microscopy. The monomer precursors, MBPA(6) and MBPA(7), exhibit two mesophases, namely, $S_A$ and $S_E$; MBPA(8) exhibits only the $S_A$ mesophase. The monomer precursors, MBPA(9), MBPA(10), MBPOE(1) and MBPOE(2), are nonliquid crystalline. The total entropy of isotropization is a measure of the extent of order present in the crystalline state and this is higher for the even monomer precursors in comparison to their odd counterparts. All polymers exhibit viscous birefringent mesophases when viewed under a polarized light microscope. In the case of polymers, it was not possible to unambiguously determine the exact molecular packing in the mesophase and assign the liquid crystalline phase to a particular type. The observation that all polymers exhibit liquid crystallinity while some of the corresponding monomers do not demonstrate stabilization of mesophases by polymer fixation[12] is in concurrence with the conclusions drawn from other liquid crystalline polymers.

## References


1. COWIE, J. M. G. — *Comprehensive polymer science*, Vol. 4, Ch. 22 (G. W. Allen and J. C. Bevington, eds), Pergamon Press, 1989, p. 377.
2. KELLER, P. — *Makromol Chem., Rapid Commun.*, 1985, **6**, 707.
3. HERALD, B., JOSEF, P. AND CHRISTIAN, W. — *Eur.. Pat. Appl.*, EP 307701, March 1989, CA 111:P176301y, (Bayer, AG).
4. HERALD, B., JOSEF, P. AND CHRISTIAN, W. — *Eur. Pat. Appl.*, EP 284,953, Oct. 1988, CA 110:P194759n, (Bayer, AG).
5. MENGER, F. M. — *Top. Curr. Chem.*, 1986, **36**, 1.
6. NEWKOME, G. R. AND MOOREFIELD, C. N. — *Mesomolecules: From molecules to materials* (G. D. Mendenhall *et al.*, eds), Chapman Hall, 1994, Ch. 2.
7. KIM, Y. H. AND WEBSTER, O. W. — *Macromolecules*, 1992, **25**, 556.
8. KIM, Y. H. AND WEBSTER, O. W. — *J. Am. Chem. Soc.*, 1990, **112**, 4592.
9. TOMALIA, D. A. AND DURST, H. D. — *Topics Curr. Chem.* (E. Weber, ed.), 1993, **165**, 193.
10. PEPPAS, N. A. AND LANGER, R. — *Science*, 1994, **263**, 1715.
11. SWIFT, G. — *Acc. Chem. Res.*, 1993, **26**, 105.
12. FINKELMAN, H. AND REHAGE, G. — *Adv. Polym. Sci.*, 1984, **60**, 113.

Thesis Abstract (Ph. D.)

**Synthetic investigations in sesquiterpenoids** by D. Vijay Kumar
Research supervisor: Prof. A. Srikrishna
Department: Organic Chemistry

## 1. Introduction

Sesquiterpenoids, among natural products, hold special appeal to synthetic chemists, as they provide fertile ground for developing and testing new synthetic strategies because of the phenomenal structural diversity present in them.[1] The present work describes the total synthesis of some sesquiterpenes such as $\alpha$-pinguisene and pingusenol, both in racemic and chiral forms, and dihydro derivatives of erythrodiene and spirojatamol in chiral form. For convenience the thesis is divided into two parts, viz. (i) Synthetic approaches to racemic and chiral pinguisanes and (ii) Enantiospecific synthesis of (+)-dihydroerythrodiene, (+)-dihydrospirojatamol and (+)-dihydro-*epi*-spirojatamol.

## 2. Synthetic approaches to racemic and chiral pinguisanes

Formal total synthesis of (±)-pinguisenol (**1**)[2] and (±)-α-pinguisene (**2**)[3] was achieved from allyl alcohol (**3**), which was obtained from Hagemann's ester (**4**). The two vicinal quaternary

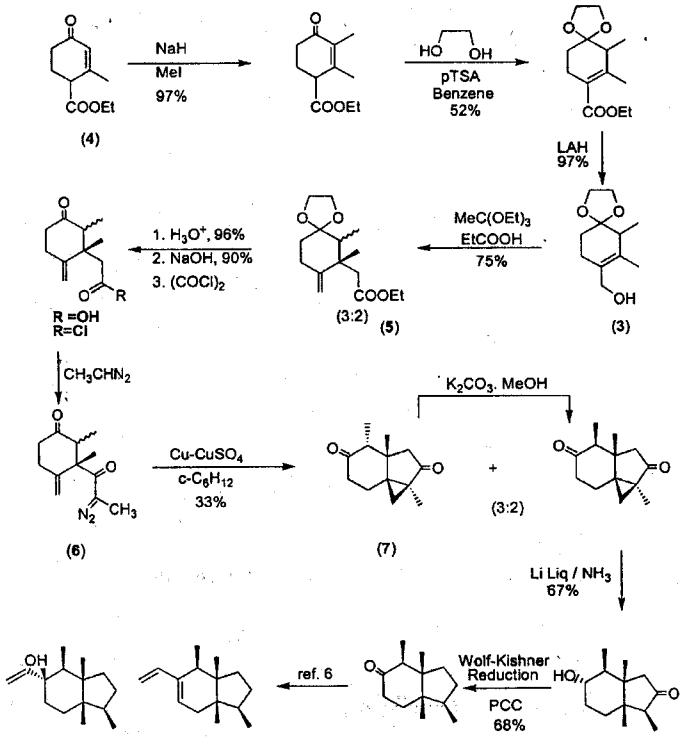


Scheme 1.

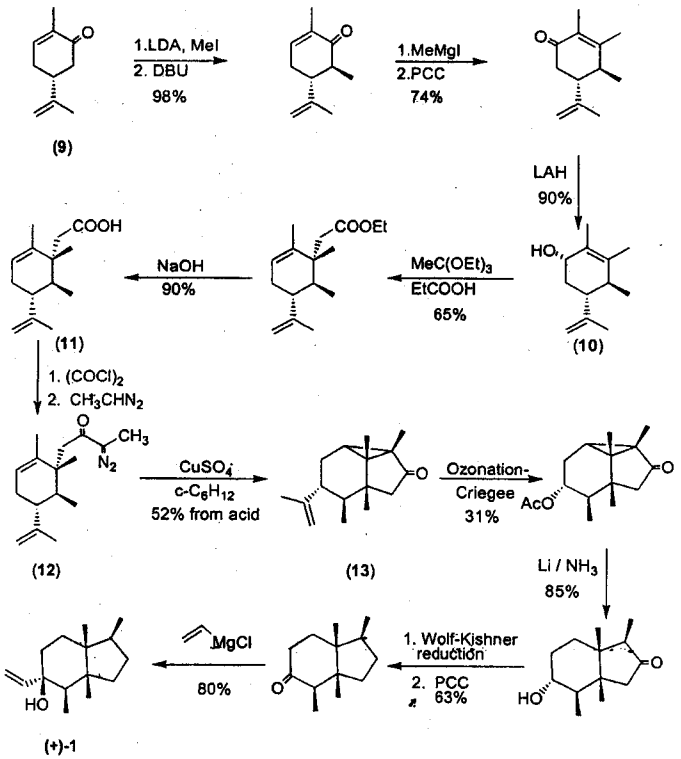


Scheme 2.

carbon atoms in pinguisanes were created employing a combination of Claisen rearrangement (**3**→**5**) and intromolecular diazo ketone cyclopropanation reactions (**6**→**7**).[4] Regiospecific cleavage of the cyclopropane ring[5] followed by functional group modifications transformed the tricyclic ketone (**7**) into Schinzer's ketone[6] (**8**), precursor of (±)-pinguisenol (**1**) and (±)-α-pinguisene (**2**) (Scheme 1).[7] For the synthesis of chiral (+)-pinguisenol (**1**), (*R*)-carvone (**9**) was chosen as the starting material, identifying the isopropenyl group as a masked hydroxy group. The allyl alcohol (**10**), obtained in four steps from (*R*)-carvone (**9**), was transformed into the acid (**11**) via orthoester Claisen rearrangement. Intramolecular cyclopropanation of the diazo ketone (**12**) derived from the acid (**11**) furnished the tricyclic compound (**13**). Degradation of the isoropenyl group in **13** followed by functional group manipulations led to (+)-pinguisenol (**1**), the optical antipode of naturally occurring (–)-pinguisenol (**1**) (Scheme 2).[8] During the synthetic studies on chiral pinguisanes, a novel fragmentation-based approach to chiral bicyclo[3.3.1]nonenies (**14**) was unraveled. Treatment of the tricyclic alcohol (**15**) with methane sulfonyl chloride and pyridine furnished bicyclo[3.3.1]nonenes (**14**), via a homo 1,4-elimination reaction and it was further generalized with a few other derivatives[9] (Scheme 3).

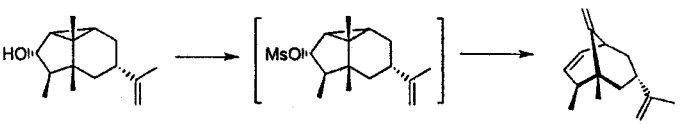


Scheme 3.

### 3. Enantiospecific synthesis of (+)-dihydroerythrodiene, (+)-dihydrospirojatamol and (+)-dihydro-*epi*-spirojatamol

Enantiospecific synthesis of dihydro derivatives of erythrodiene (**17**), spirojatamol (**18**) and *epi*-spirojatamol (**19**) is described in the second chapter. Stereochemically pure dihydrocarvone **20**) was converted into spiro[4.5]decane system (**21**) employing Claisen rearrangement (**22**→**23**), Wacker oxidation (**23**→**24**) and intramolecular aldol condensation (**24**→**21**) sequence. The spiroenone (**21**) was further elaborated to (+)-dihydroerythrodiene (**17**), (+)-dihydrospirojatamol (**18**) and (+)dihydro-*epi*-spirojatamol (**19**)[10] (Scheme 4).

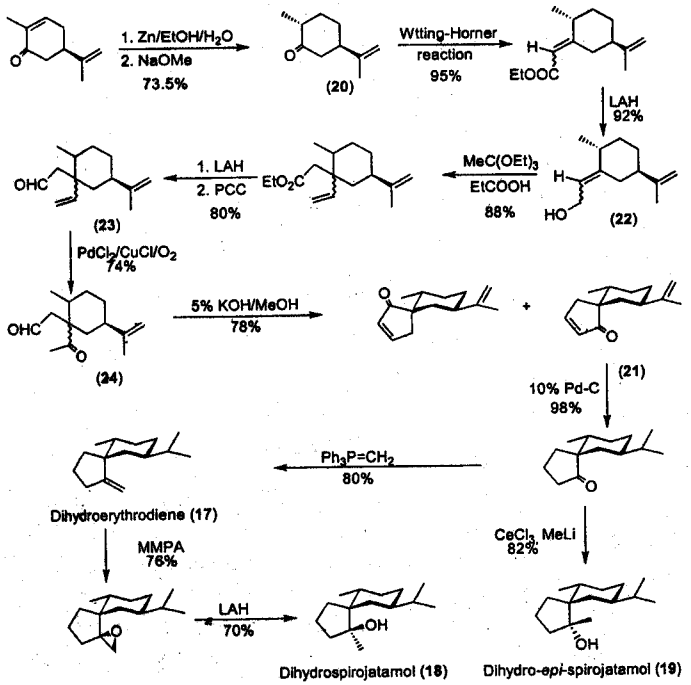


Scheme 4.

## References


1. HEATHCOCK, C. H. — *The total synthesis of natural products*, Vol. 2 (J. ApSimon, ed.), Wiley, 1973.
2. ASAKAWA, Y., TOYOTA, M. AND ARATANI, T. — *Tetrahedron Lett.*, 1996, 3619.
3. ASAKAWA, Y., TOYOTA, M. AND TAKEMOTO, T. — *Phytochemistry*, 1978, **17**, 457.
4. SRIKRISHNA, A. AND KRISHNAN, K. — *J. Chem. Soc., Perkin Trans. 1*, 1993, **58**, 7751.
5. a. STORK, G., UYEO, S., WAKAMATSU, T., GRIECO, P. AND LABOVITZ, J. — *J. Am. Chem. Soc.*, 1971, **93**, 4949.
   b. DAUBEN, W. G. AND DEVINY, E. J. — *J. Org. Chem.*, 1974, **39**, 2217.

6. a. SCHINZER, D., RINGE, K., JONES, P. G. AND DORING, D. *Tetrahedron Lett.*, 1995, **36**, 4051.

b. SCHINZER, D. AND RINGE, K. *Tetrahedron*, 1996, **52**, 7475.

7. SRIKRISHNA, A. AND VIJAYKUMAR, D. *J. Chem. Soc., Perkin Trans. 1*, 1997, 3295 and *J. Chem. Soc., Perkin Trans. 1*, 1999, 1265.

8. SRIKRISHNA, A. AND VIJAYKUMAR, D. *Tetrahedron Lett.*, 1998, **39**, 4901.

9. SRIKRISHNA, A. AND VIJAYKUMAR, D. *Tetrahedron Lett.*, 1998, **39**, 5833.

10. SRIKRISHNA, A., VIJAYKUMAR, D. AND JAGADEESWAR REDDY, T. *Tetrahedron*, 1997, 1439.

Thesis Abstract (Ph. D.)

**Molecular insights into the architecture and assembly of physalis mottle virus** by Mira Sastri

Research supervisor: Prof. H. S. Savithri

Department: Biochemistry

## 1. Introduction

Viral assembly is an intricate process involving protein folding, assembly and interaction with nucleic acids. It is an important event in the life cycle of the virus and has received increasing attention over the past few years with an appreciation of the complexities of the problem. The great simplicity of the viruses, in comparison to cells makes them invaluable tools in the elucidation of gene structure and function, as well as the assembly of biological structures. In order to understand the molecular details of assembly one must also have an in-depth knowledge on the architecture of the viruses. In most instances, the assembly mechanisms *in vitro* are studied by reconstitution of isolated capsid protein with isolated nucleic acids. Such studies have led to the identification of intermediates in the assembly of a helical virus such as tobacco mosaic virus, but in the case of icosahedral viruses, it is usually an all or none phenomenon. Further, in the case of viruses stabilized predominantly by protein–protein interactions, harsh conditions are required to disrupt the virions and these render the isolated protein assembly incompetent. Most recently, the mechanism of assembly of viruses is being unraveled employing capsid proteins and their mutants expressed in bacterial systems by using a combination of biophysical and crystallographic methods. PhMV consists of a monopartite single-stranded positive-sense RNA genome encapsidated in an icosahedral shell of 180 identical subunits (subunit $M_r$ 22 kDa). Purified preparations of PhMV contain two kinds of particles, the intact nucleocapsids and the empty capsids that can be separated by sucrose gradient centrifugation into denser bottom (PhMV-B) component and lighter top (PhMV-T) component, respectively. *In vitro* assembly of any tymovirus from isolated components has not been reported so far. Therefore, we resorted to molecular biological tools to study the assembly process of PhMV.

In this work, the coat protein gene of PhMV was overexpressed in *Escherichia coli* and the recombinant protein was characterized. The role of the amino and carboxy termini in capsid

assembly was elucidated and the residues involved in intersubunit interactions were determined.

## 2. Materials and methods

The cDNA clone TA 51 was used in PCR to generate the recombinant and deletion constructs. Site-directed mutagenesis was performed using the megaprimer method[1] and the mutations were confirmed by Sanger's dideoxy method.[2] Purification of native, recombinant and the mutant capsids were performed according to Sastri *et al.*[3] The mutant proteins were electroblotted onto Nylon membrane[4] and the N-terminal sequence was determined using Shimadzu gas-phase sequenator PSQ-1. The sedimentation coefficient of the recombinant and mutant capsids was determined by the method of Brakke and van Pelt.[5] The capsids were stained with uranyl acetate and viewed under the electron microscope. The diameter of the particles was measured by Wild Heerburg polarizing microscope. The recombinant and mutant capsids were characterized by agarose gel electrophoresis, HPLC, ELISA and Western blotting techniques. RNA was extracted from the capsids using phenol-chloroform method and used in RNA-slot blot experiments.[6] *In-vitro* translation experiments of the RNA isolated from the native and recombinant capsids were performed by using Amsheram ECL *in-vitro* translation system.

## 3. Results and discussion

Previously, the coat protein gene had been expressed in our laboratory in the vector pKK 223-3.[7] However, the recombinant protein was in the inclusion bodies and hence was difficult to purify it. The coat-protein gene was, therefore, cloned into other expression vectors and preliminary characterization of the overexpressed protein was carried out. The coat protein gene was cloned in pET 3d vector and overexpressed in B121 (DE3) cells. The recombinant protein (PhCP) was found to self-assemble into capsids *in vivo*. The purified recombinant capsids had an apparent S value of 56.5 and a diameter of $29 \pm 2$ nm. These capsids were as stable as PhMV-T to high salt (2 M KCl), several cycles of freezing and thawing and to a wide range of pH (4.2–9.0). Urea denaturation studies on these capsids showed that the recombinant capsids were stable up to 4 M urea in contrast to PhMV-B, which was stable only up to 3 M urea. These capsids were also capable of encapsidating their own mRNA which was messenger active.

Earlier studies, using monoclonal antibodies, had shown that the residues 22–36, were exposed in the intact virus and RNA–protein interaction was mediated through Lys 10.[8] In order to delineate further the role of the N- and C-terminal residues in capsid assembly, six amino terminal deletion clones lacking the first 11, 26, 30, 34, 35 and 39 amino acid residues and two carboxy terminal deletions lacking the last 5 and 10 amino acid residues were constructed and overexpressed. The proteins lacking N terminal 11 (PhCPN1), 26 (PhCPN2) and 30 (PhCPN3) amino acid residues self-assembled into $T = 3$ capsids *in vivo* as evident from electron microscopy, ultracentrifugation and agarose gel electrophoresis. The PhCP, PhCPN1, PhCPN2 and PhCPN3 capsids were as stable as the empty capsids formed *in vivo* and encapsidated a small amount of mRNA. The subtle conformational changes in the various deletion capsids were probed using the monoclonal antibody PA3B2. The monoclonal antibody PA3B2 that recognizes the epitope within region 22–36 failed to react with PhCPN2 capsids while it recognized

the recombinant and PhCPN1 capsids. Thus, the epitope for the MAb mapped between the residues 22–26. Disassembly of the capsids upon treatment with urea showed that PhCPN2 capsids were the most stable. The deletion of 34, 35 and 39 amino acids rendered the protein insoluble. In the recently determined structure of PhMV, it is observed[9] that the $\beta$-barrel begins at residue 31 and deletions beyond 31 residues would perhaps interfere in the folding of the protein and lead to insoluble aggregates. These results demonstrate that N-terminal 30 amino acid residues are not essential for T = 3 capsid assembly in PhMV. In contrast, both the proteins lacking the C-terminal 5 and 10 amino acid residues were present only in the insoluble fraction and could not assemble into capsids suggesting that these residues are crucial for folding and assembly of the particles.

Assembly intermediates of icosahedral viruses are usually transient and are difficult to identify. Site-specific and deletion mutants of the coat protein gene of PhMV were used to delineate the role of specific amino acids in the assembly of the virus and to identify intermediates in this process. Single C-terminal (N188) deletion mutant protein of PhMV and site-specific mutants H69A, C75A, W96A, D144N, D144N-T151A, K143E and N188A were constructed in pET 3d and expressed in BL21 (DE3) pLysS. The mutations were designed based on sequence comparison with other tymoviruses and on their uniqueness. All the site-specific mutants except N188A went into the insoluble fraction. Several methods of solubilization were tried but most of them were unsuccessful. Therefore, the mutants as well as the wild-type coat protein was recloned into pRSET B vector. This vector has an advantage of the histidine tag that would help in purifying the proteins and it was hoped that the additional amino acids at the N-terminus would help in obtaining soluble proteins. Interestingly, the coat protein (pR PhCP) expressed using pRSET B vector with an additional 41 amino acids at the N-terminus also assembled into T = 3 particles that were more compact and had a smaller diameter. These results demonstrate that the amino terminal segment is flexible and either the deletion or addition of amino acids at the N-terminus does not affect T = 3 capsid assembly. In contrast, the deletion of even a single amino acid from the C-terminus (PhN188$\Delta$1) resulted in capsids that were unstable. These capsids disassembled to a discrete intermediate with a sedimentation coefficient of 19.4 S. But the replacement of C-terminal asparagine 188 by alanine led to the formation of stable capsids. The C75A and D144N mutant proteins also assembled into capsids that were as stable as the pR PhCP suggesting that C75 and D144 are not crucial for the T = 3 capsid assembly. pR PhW96A and pR PhD144N-T151A mutant proteins failed to form capsids and were present as heterogeneous aggregates. The pR PhK143E mutant protein behaved in a manner similar to the C-terminal deletion protein in forming unstable capsids. The intermediate with an *s* value of 19.4 was the major assembly product of pR PhH69A mutant protein and could correspond to a 30 mer. It is possible that the assembly or disassembly is arrested at a similar stage in pR PhN188$\Delta$1, pR PhH69A and pR PhK143E mutant proteins.[10] The data are discussed in the light of the recently determined crystal structures of PhMV and TYMV.

The results demonstrate that the N-terminal arm shown to be ordered in all the subunits of PhMV in the crystal structure[9] is flexible and can assume different conformations in solution. Stable T = 3 capsids can be formed upon either deletion of 30 amino acids or the addition of 41 amino acids at the N-terminus. The C-terminal Asn, involved extensive quasi 2-fold and quasi 3-fold contacts, is crucial to the assembly of the virus. For the first time, a sub-assembly intermediate was identified and characterized in the present study.

## References


1. LANDT, O., GRUNERT, H. AND HAHN, U. — A general method for rapid site-directed mutagenesis using polymerase chain reaction, *Gene*, 1990, **96**, 125–128.
2. SANGER, F., NICKLEN, S. AND COULSON, A. R. — DNA sequencing with chain terminating inhibitors, *Proc. Natn. Acad. Sci. USA*, 1977, **74**, 5463–5467.
3. SASTRI, M. *et al.* — Assembly of Physalis mottle virus capsid protein in *Escherichia coli* and role of amino and carboxy termini in the formation of icosahedral particles, *J. Mol. Biol.*, 1997, **272**, 541–552.
4. MATSUDAIRA, P. — Sequence from picomole quantities of proteins electroblotted onto polyvinyllidene difluoride membrane, *J. Biol. Chem.*, 1987, **262**, 10035–10038.
5. BRAKKE, M. K. AND NANCY VAN PELT — Linear-log sucrose gradients for estimating sedimentation coefficients of plant viruses and nucleic acids, *Anal. Biochem.*, 1970, **38**, 56–64.
6. SAMBROOK, J., FRITISCH, E. F. AND MANIATIS, T. — *Molecular cloning: a laboratory manual*, Cold Spring Harbor Laboratory, Cold Spring Harbor, NY, 2nd edn, 1989.
7. KEKUDA, R. — *Mapping of antigenic determinants and regions of RNA–protein interactions in physalis mottle virus*. Ph. D. Thesis, Indian Institute of Science, Bangalore, 1993.
8. KEKUDA, R., KARANDE, A. A., JACOB, A. N. K. AND SAVITHRI, H. S. — Architecture of Physalis Mottle Tymovirus as probed by monoclonal antibodies and cross-linking studies, *Virology*, 1993, **193**, 959–966.
9. SRI KRISHNA, S. *et al.* — Three-dimensional structure of physalis mottle virus: implications for the viral assembly, *J. Mol. Biol.*, 1999, **289**, 919–934.
10. SASTRI, M., REDDY, D. S., SRI KRISHNA, S., MURTHY, M. R. N. AND SAVITHRI, H. S. — Identification of a discrete intermediate in the assembly/disassembly of Physalis mottle tymovirus through mutational analysis, *J. Mol. Biol.*, 1999, **289**, 905–918.


Thesis Abstract (Ph. D.)

**Immunochemical characterization of glycoprotein allergens from the pollens of *Parthenium hysterophorus* and *Helianthus annuus* (sunflower) and studies on the induction of oral tolerance in a murine mode** by K. A. Ganesh

Research supervisor: Prof. P. V. Subbarao

Department: Biochemistry

## 1. Introduction

Allergy is the most prevalent disorder mediated by the IgE class of antibodies and inflicts almost 10% of the world population. Inhalant allergens including pollens, dust mites, animal danders and fungal spores have been well documented as the cause for the type-I immediate hypersensitivity reactions in the airways.[1] The South American *Compositae* weed, *Parthenium hysterophorus* is a world-wide allergen responsible for high incidence of IgE-mediated type-I hypersensitive reactions in sensitive individuals resulting in seasonal and perennial allergic

rhinitis. Varying titers of *Parthenium* pollen-specific IgE antibodies were detected in the sera of *Parthenium*-sensitive patients by AB-micro-ELISA.[2] Sunflower (*Helianthus annuus*), another member of the family *Compositae*, is an important cash crop. Persons employed in sunflower fields have often been observed to complain about symptoms of rhinitis after exposure to the pollen. In addition, these patients show positive skin prick reaction and serum IgG/IgE levels to both *Parthenium* and sunflower pollen extracts. Competitive ELISA inhibition experiments revealed that *Parthenium* pollen extracts could completely inhibit the binding of IgE antibodies in the sera of *Parthenium*-sensitive individuals to sunflower pollen. Hence, it is important to study the nature of cross-reactivity between *Parthenium* and sunflower pollen allergens.

## 2. Experimental and discussion

Earlier studies from our laboratory have led to the purification of the acidic, hydroxyproline-rich 31 kDa glycoprotein allergen, Par h 1[3] and the 14 kDa pan allergen, Profilin. The present investigation describes the identification, purification and immunochemical characterization of a 45 kDa glycoprotein from sunflower, as the allergen cross-reacting with Par h 1. The 45-kDa allergen, designated as Hel a 1, was purified to homogeneity by a combination of ion-exchange chromatography and HPLC. The purified allergen was recognized by IgE antibodies from the sera of most of the *Parthenium*-sensitive individuals. This binding could be inhibited by Par h 1. Hel a 1 was found to be heavily glycosylated (48% w/w carbohydrate). Results obtained from periodate oxidation and pronase digestion of Hel a 1 revealed that sugar groups covalently linked to polypeptide backbone of Hel a 1 contribute significantly to IgE-binding properties. In addition, the N-terminal sequence of Hel a 1 was found to be completely identical to Par h 1. Periodate-oxidized total *Parthenium* and sunflower extracts lose their ability to elicit skin-prick reactivity in sensitive individuals, hence it may act as a potential candidate for allergen-specific immunotherapy.

Immunoblot analysis of total *Parthenium* pollen extract revealed the presence of many IgE-binding allergens ranging from 45 to 14 kDa. Although most of the IgE binding towards total *Parthenium* pollen extract is accounted for by the acidic glycoprotein, Par h 1 (which is bound to DEAE-Sephacel ion exchange matrix), the DEAE-unbound fraction, comprising basic protein allergens (pI range greater than 8) also showed considerable IgE-binding activity. Immunoblot analysis of basic protein allergens with sera from sensitive individuals revealed intense binding of IgE antibodies to a 31-kDa glycoprotein. This protein was subsequently purified to homogeneity through FPLC gel filtration column, and designated as Par h 2. Similar to Par h 1, the IgE-binding epitopes of Par h 2 were also found to be carbohydrate in nature. ELISA inhibition and immunoblot inhibition assays of Par h 2 with the acidic glycoprotein allergen Par h 1 revealed the extensive cross-reactivity between these two allergens. N-terminal analysis and other immunochemical properties of Par h 2 however showed that the polypeptide backbone is different from Par h 1. Periodate-insensitive and pronase-susceptible anti-Par h 1 rabbit IgG antibodies bind very weakly to Par h 2 suggesting that the extensive cross-reactivity between acidic and basic major allergens is mainly due to similar IgE (human)-binding carbohydrate determinants of Par h 1 and Par h 2. ELISA inhibition assay and *in-vivo* skin-prick test performed with purified allergens revealed that Par h 2 is more potent as an allergen compared to Par h 1 in terms of both *in vitro* and *in vivo* IgE binding. Sodium *meta-*

periodate-modified Par h 1 and Par h 2 completely lose their capacity to elicit positive skin-prick reactivity in patients sensitive to *Parthenium* pollen.

Carbohydrate analysis of TFA-treated Par h 1 through HPLC revealed the exclusive presence of arabinose sugar. However, free arabinose failed to inhibit IgE antibody binding to native allergen *in vitro*, suggesting the presence of complex higher order structure of arabinose linkage at many hydroxyproline residues.

PAS staining and lectin overlay assay of total *Parthenium* pollen proteins revealed the presence of many glycoprotein allergens with relative molecular weights of 42, 29, 21 and 19 kDa. The 42 and 29 kDa proteins were purified by Con A affinity chromatography and were found to co-elute by α-methylmannoside. The 19 and 21 kDa allergens bind to cation exchange CM cellulose column. All these proteins have been categorized under group II allergens based on their common Con A-binding properties. Further, these allergens were found to possess periodate sensitive, IgE-binding carbohydrate determinants, but could not be inhibited by either Par h 1 or Par h 2 suggesting the existence of distinct IgE-binding carbohydrate epitopes.

The administration of soluble antigen through the oral route has been described as a means of inducing antigen-specific systemic immune tolerance to subsequent parenteral antigen challenge.[4, 5] The induction of specific oral tolerance provides a potential strategy for the treatment of allergic diseases.[6] The effect of oral administration of *Parthenium* pollen extract on the humoral and cellular immune responses of BALB/c mice was studied by feeding high doses of pollen extract prior to parenteral challenge with alum-adsorbed *Parthenium* pollen antigen. Both IgG and IgE antibodies were found to be down-regulated in the mice fed with pollen extract as compared to saline-treated control animals. Splenocytes from the mice administered with pollen extract through oral route showed reduction in proliferative responses studied by *in vitro* recall assay. The tolerance effect of suppressed humoral and cellular immune reponse in mice fed orally with pollen extract was maintained even after secondary parenteral antigen challenge.

Since allergy to *Parthenium* is chronic, it is of interest and of obvious relevance to see whether oral tolerance can be achieved in an ongoing immune response. Adjuvant free intranasal immunization of mice with protein antigens showed to result in specific immune response.[7] In the current study, a murine model was developed in BALB/c by adjuvant free intranasal immunization (i.n.), of *Parthenium* pollen extract. i.n. with native antigen resulted in Th2 type of immune response dominated by high amounts of antigen-specific IgG1 and IgE antibodies. Secondary i.n. immunization results in heightened IgG and IgE antibody titers as compared to saline-treated control mice. In order to see the effect of oral feeding on an already established allergen-specific ongoing immune response, the mice were intranasally sensitized with pollen extract and subsequently fed with high doses of the pollen extract. While the oral feeding of pollen extract resulted in the inhibition of IgE antibody production after secondary intranasal treatment, the IgG antibody titres remained unchanged. Upon *in-vitro* recall with native antigen the splenocytes from the mice which received oral *Parthenium* secreted more amount of IFN-γcompared to saline-fed control animals. These studies suggest the possible occurrence of immunomodulation of the responses following oral administration rather than the induction of active suppression.

## References


1. KAY, A. B. — Asthma and inflammation, *J. Allergy Clin. Immunol.*, 1991, **87**, 893.
2. SRIRAMARAO, P., NAGPAL, S., SUBBARAO, B. S., PRAKASH, O. AND SUBBARAO, P. V. — Immediate hypersensitivity to *Parthenium hysterophorus*. II. Clinical studies on the prevalence of *Parthenium hysterophorus*, *Clin. Expl Allergy*, 1996, **21**, 55.
3. GUPTA, N., MARTIN, B. M. METCALFE, D. D. AND SUBBARAO, P. V. — Identification of a novel hydroxyproline-rich glycoprotein as the major allergen in *Parthenium* pollen, *Allergy Clin. Immunol.*, 1996, **98**, 903.
4. CHALLACOMBE, S. J. AND TOMASI, T. J. — Systemic tolerance and secretary immunity after oral immunization, *J. Expl. Med.*, 1980, **152**, 1459.
5. STROBER, W., KELSAL, B. AND MARTH, T. — Oral tolerance, *J. Clin. Immunol.*, 1998, **18**, 1.
6. NGAN, J. AND KIND, L. S. — Suppressor T cells for IgE and IgG in Peyer's patches of mice made tolerant by the oral administration of ovalbumin, *J. Immunol.*, 1978, **120**, 861.
7. RENZ, H. *et al.* — Aerosolized antigen exposure without adjuvant causes increased IgE production and increased airway responsiveness in the mouse, *J. Allergy Clin. Immunol.*, 1992, **89**, 1127.


Thesis Abstract (Ph. D.)

**Molecular and immunological approaches to understand the basis for pathogenesis of *Mycobacterium tuberculosis*** by Amara Rama Rao
Research supervisor: Prof. S. Vijaya
Department: Microbiology and Cell Biology

## 1. Introduction

Tuberculosis continues to be a major health problem worldwide. The causative agent *Mycobacterium tuberculosis* (M. tb) accounts for nearly three million deaths and eight million fresh cases every year. The emergence of multi-drug resistant strains and the widespread occurrence of TB among AIDS patients make for an alarming situation. The unsatisfactory protection offered by the live attenuated vaccine *Mycobacterium bovis* bacillus Calmette-Guerin (BCG) calls for the development of a safe and more effective vaccine. Despite two decades of extensive research, the biology of the organism is not well understood.

*Mycobacterium tuberculosis* has a unique ability to infect and multiply within the macrophages, which constitutes a major component of the host's innate immune system. This capability has partly been attributed to the inhibition of fusion between the phagosomes containing M. tb with lysosomes, perhaps by selective exclusion of proton ATPase from these phagosomes as shown by David Russell, resulting in lack of acidification of these vacuoles. However, the molecular mechanisms by which the organism is able to bring about these effects are not known. We hypothesized that a battery of genes differentially turned on by the bacte-

rium only in the host in response to the hostile macrophage environment, but not expressed when the bacterium is grown in synthetic media *in vitro*, may contribute to its survival in the host. Once identified, manipulation of these differentially expressed genes may help to devise strategies for arresting the growth of this organism in the host.

T cells but not antibodies have been shown to be important for protection against tuberculosis. Human T cell lines reactive to M. tb sonicates respond weakly to live bacteria. In mice also, live M. tb, but not dead organisms, protected against a challenge dose of virulent M. tb.. These observations have led to the intriguing possibility that living mycobacteria elaborate antigens, perhaps secreted into the extracellular environment of the bacilli, the immune response to which leads to protection. Alternatively, it is believed that the expression of certain antigens responsible for protective immunity may be turned on or upregulated in bacilli actively replicating *in vivo*, namely, within the host environment. The work summarized below represents an attempt to address the above-mentioned aspects of tuberculosis: firstly, to attempt an understanding of the molecular basis of its pathogenesis, and secondly to identify protective antigens of the organism.

## 2. Experimental

### 2.1. *Construction and analysis of a genomic DNA expression library of Mycobacterium tuberculosis*

During the progression of tuberculosis, T cell responses are suppressed whereas the B cell responses are augmented with a concomitant increase in antibody titers in TB patients. The inability of antibodies to confer protection against tuberculosis notwithstanding, they may serve as valuable reagents, by virtue of their ability to recognize B-cell epitopes in the antigens relevant for protection and for altering host immune responses. We therefore constructed a genomic DNA expression library for a field isolate of *M. tuberculosis* in the lambda ZAP II expression vector and screened this library with pooled sera obtained from chronically infected TB patients. This screen resulted in identification of 176 recombinants (representing nearly 40 unique genes of the bacterium), which are immunodominant during the active phase of the disease.[2] We wished to find out if serum obtained from patients in early stages of tuberculosis would recognize all 176 recombinants that were originally identified using serum from chronically infected patients. We observed interesting differences in the reactivity of antigens specified by some of these recombinants to the two serum pools. Some recombinants showed preferential reactivity to either late or early phase sera. This is suggestive of alterations either in the expression of these proteins or in the host immune response to these proteins as the disease progresses from establishment to maintenance phase.

### 2.2. *Differential immunogenicity of novel Mycobacterium tuberculosis antigens*

In order to see whether any of the antigens we had identified were made only in the host we raised antibodies to total *M. tuberculosis* sonicate (grown in synthetic medium *in vitro*) in three different strains of mice. *E. coli* lysates obtained from TB patient serum–reactive recombinants were immunoblotted to pools of both TB patient sera and mouse sera at equivalent titers. Only 10 of 26 recombinant proteins tested showed reactivity to the pooled mouse sera whereas all the recombinant proteins reacted well as expected with the pooled TB patient sera. Both sera

however showed good reactivity to total *M. tuberculosis* sonicates. Similar results were obtained when antisera obtained from guinea pigs infected with live *M. tuberculosis* as well as immunized with sonicated preparations of *M. tuberculosis* were compared for reactivity to the recombinant proteins. These results suggest that actively replicating bacilli in the human or guinea pig host elicit antibodies to a unique category of proteins/epitopes, only a minority of which are immunodominant in killed bacillary preparations. In order to see if these proteins are made when the bacterium is grown in synthetic medium, antisera were raised in mice to seven recombinant proteins that were not recognized by pooled mouse sera, and Western blotted to total M. tb sonicate. All the seven proteins were present in significant amounts in *M. tuberculosis* grown *in vitro*. This raises the possibility that there may be differences in the presentation of the same antigens to the host immune system when these antigens are elaborated by living bacilli as opposed to being derived from killed bacilli, resulting in differential immunogenicity.[3]

### 2.3. *Characterization of novel immunodominant antigens of Mycobacterium tuberculosis*

We have further characterized these seven recombinant proteins which showed differential immunogenicity. The nucleotide sequences of these seven recombinants were compared to all entries in the database. Two clones represented the *M. tuberculosis* homologues of FtsH and aminoimidazole ribotide synthase. The sequence of a third recombinant clone showed low level similarity to enoyl-CoA hydratase. The sequences of the remaining four clones had no homology to any entries in the database. We studied the distribution of these seven genes in other pathogenic and nonpathogenic mycobacteria. In addition, the subcellular localization of the respective proteins and their hydrophobicity as judged by ability to partition into Triton X-114 was determined.[4]

### 2.4. *T cell responses to novel antigens of M. tuberculosis*

T cell responses have been shown to mediate protection in tuberculosis. We were interested to see whether any of the immuno-dominant antigens we had identified using B cell responses could elicit T cell response in healthy contacts (individuals exposed but not diseased) and in tuberculosis patients. Among the 11 antigens tested, two elicited a good T cell response only in healthy contacts but not in patients. We found that the responding cells produced TNF-$\alpha$, IFN-$\gamma$, and IL-12 but not IL-4, indicative of a Th1 phenotype. By depletion of specific T cell subsets, we also showed that the responding cells were CD4 positive. Several deletions of these proteins have been made and the epitopes have been mapped to a small stretch of the protein. We are currently in the process of determining the ability of these T cells to protect against a challenge dose of virulent *M. tuberculosis* in a guinea pig animal model by vaccination in the form of naked DNA.

### 2.5. *Specific polyadenylation and purification of messenger RNA from prokaryotes*

Subtractive hybridization and differential display reverse transcription PCR (DDRT-PCR) have been widely used to identify differentially expressed genes. However, use of these techniques with prokaryotic systems has been difficult because the former calls for the availability of messenger RNA in a pure form whereas the latter requires the presence of a poly (A) tail at

the end of message. We have developed a method to specifically polyadenylate messenger RNA from prokaryotes.[5] We hypothesized that in the form of polysomes the 3′ ends of messenger RNA alone will be available for polyadenylation. We showed using *E. coli* as a model system, that messenger RNA can be specifically polyadenylated *in vitro* by yeast poly (A) polymerase and subsequently purified using oligo dT affinity chromatography. We subsequently carried out DDRT-PCR analysis of *E. coli* messages obtained from uninduced and high salt-induced conditions to identify salt-induced genes of this organism. Several clones thus identified are in the process of being characterized.

### 2.6. *Identification of differentially expressed genes of Mycobacterium tuberculosis*

As mentioned earlier, differentially expressed genes of the bacterium as well as the host may play an important role in the pathogenesis of tuberculosis. In order to identify these genes we have carried out subtractive hybridization of messages obtained from M. tb grown in synthetic medium as well as uninfected guinea pig tissue, from messages of M. tb-infected guinea pig tissue. Subtracted messages were amplified by PCR and subsequently cloned in pBluscript vector. These clones were screened with $^{32}P$ labeled probes obtained by reverse transcription of total messages either from infected or uninfected guinea pig tissue or M. tb grown in synthetic medium, to eliminate false positives and to confirm the authenticity of their differential nature. In this screen, we have identified several clones and are currently in the process of characterizing them.

## References


1. RAMA RAO, A. AND VIJAYA, S. — An approach for studying the mediators of pathogenesis in *Mycobacterium tuberculosis, J. Biosci.*, 1996, **21**, 421–423.
2. RAMA RAO, A. AND VIJAYA, S. — Analysis of a genomic DNA expression library of *Mycobacterium tuberculosis* using tuberculosis patient sera: Evidence for modulation of host immune response, *Infect. Immun.*, 1996, **64**, 3765–3771.
3. RAMA RAO, A. AND VIJAYA, S. — Differential immunogenicity of novel *Mycobacterium tuberculosis* antigens derived from live versus dead bacilli, *Infect. Immun.*, 1997, **65**, 4880–4882.
4. RAMA RAO, A., SHANTI, S. AND VIJAYA, S. — Characterization of novel immunodominant antigens of *M. tuberculosis, Microbiology*, 1998, **144**, 1197–1203.
5. RAMA RAO, A. AND VIJAYA, S. — Specific polyadenylation and purification of total messenger RNA from *Escherichia coli, Nucleic Acids Res.*, 1997, **25**, 3465–3470.


Thesis Abstract (Ph. D.)

**Photoluminescence of some transition and rare earth metal ions doped aluminates and aluminosilicate phosphors prepared by wet chemical methods** by Mohandas Nayak

Research supervisor: Prof. T. R. N. Kutty
Department: Materials Research Centre

## 1. Introduction

Inorganic photoluminescent materials have gained tremendous importance because of their use in energy-efficient fluorescent lighting.[1–6] There has been an extensive research in the area of lamp phosphors for more than a decade, which yielded phosphors with very high efficiency. The phosphors were obtained with ideal properties and different varieties of fluorescent lamps have been obtained and are currently under use.[3–6] The new generation compact fluorescent lamps yield > 120 lm/W in comparison to the 60 lm/W by the widely used halophosphate lamps. High efficiency is achieved by employing a trichromatic phosphor blend comprising three phosphors having localized emission bands in three primary colour regions: blue, green and red to feed human photoreceptor system. However, besides their high power efficiency, the use of these lamps is limited by their high cost because of the use of expensive rare earths as activators or as hosts. Another factor which contributes for the increased cost is the stringent firing conditions (~1600°C) required for the preparation of aluminate phosphors. Cost can be reduced by using low-temperature preparative routes for these phosphors and by substituting expensive phosphors with cheaper ones. In the present investigation, special emphasis has been laid on evolving an economical low-temperature synthetic method for the preparation of high-efficiency phosphors, side by side with the search for the new luminescent materials, their characterization and structure–property correlation.

For the present study, the hosts chosen are alkaline earth aluminates, alkali aluminates, aluminosilicates, alkaline earth aluminosilicates and their solid solutions, alkali aluminosilicates, aluminium hydroxides and oxyhydroxides. The activators used are $Eu^{2+}$, $Ce^{3+}$ and $Fe^{3+}$. These activators involve the f–d ($Eu^{2+}$, $Ce^{3+}$) and d–d transitions wherein the d-states are highly sensitive to the crystallochemical effects when doped in a solid. The degeneracy of d-states will be removed by the crystal field and split into 2 to 5 different energy levels depending upon the crystal field symmetry. Hence these activators are also used as luminescent probes for obtaining information about local structure.

## 2. Experimental techniques

The aluminates and aluminosilicates have been prepared by the gel-to-crystallite conversion (G–C) and hydrothermal method. The G–C method involves the reaction of hydrated alumina gel ($Al_2O_3.xH_2O$) with $A^{n+}(OH)_n$, where A = $Si^{4+}$, $Ba^{2+}$, $Sr^{2+}$, $Ca^{2+}$, $Mg^{2+}$, $Na^+$, $K^+$, $Li^+$, etc. in the presence of a hydrophilic solvent, such as ethanol, at 80–100°C for 4 to 6 h. Often, the as-prepared form is a metastable hydroxylate which acts as a precursor and decomposes on calcination to give the end product. Doping of the activator ion ($Fe^{3+}$: 0.1–0.3 mol%; $Eu^{2+}$: 1–4 mol%; $Ce^{3+}$:1–4 mol%) is done by co-precipitating with metal hydroxide gel from mixed salt solution. The G–C conversion can be schematically represented as follows:

The basic reaction mechanism involved in the hydrothermal synthesis is similar to G–C conversion but the preparative conditions differ. Hydrothermal synthesis is at low temperature (<240°C) and high pressure. The reactions have been carried out in a Teflon-lined stainless steel autoclave charged with reactants and deionised water to the required percentage fill so as to autogenerate pressure in the range 30–150 Mpa, when heated between 70°C and 300°C.

The physicochemical methods adopted for the characterization are X-ray diffraction (XRD), differential thermal analyses (DTA), thermogravimetry (TG), photoluminescence spectroscopy, electron paramagnetic resonance (EPR), nuclear magnetic resonance (NMR), infrared absorption spectroscopy and microscopic techniques like SEM and TEM.

## 3. Results and discussion

### 3.1. *Metastable phase relations and $Eu^{2+}$ luminescence of barium hexa-aluminates*

Barium hexa-aluminate phosphors were obtained by the decomposition of the G–C conversion prepared precursor $Ba_{1+x}Al_{12}O_{19+x-z/2}(OH)_z.nH_2O$ ($-0.2 < x < 0.32$; $15 < z < 20$; $.5 < n < 9$), which on decomposition above 1150°C produces monophasic barium hexa-aluminate.[7] A series of nonstoichiometric compositions are obtained represented by the general formula $Ba_{1+x}Al_{12}O_{19+x}$ ($-0.2 < x < 0.3$). Metastability of these nonstoichiometric phases is evident from the splitting of (00*l*) reflections in X-ray diffraction pattern on heat treatment above 1600°C, indicating the subsolidus decomposition to $0.82BaO.6Al_2O_3$ and $1.32\ BaO.6Al_2O_3$. The nonstoichiometry in these compounds is accommodated by extensive distribution of the blocking effects and structural intergrowths as revealed by high-resolution electron microscopy. The metastable Ba-hexa-aluminates doped with $Eu^{2+}$ exhibit predominantly 436 nm emission for all the $x$ values. The quantum efficiency is maximum for the composition $1.32BaO{\cdot}6Al_2O_3$ and is enhanced by partial substitution with CaO and $B_2O_3$. $Eu^{2+}$ luminescence is associated with transition from $4f^65d$ excited state to $4f^7$ ground state. The strong emission is due to the electric dipole-allowed d-f transition. Luminescence characteristics of $Eu^{2+}$ are changed when aliocompositional additives such as MgO are substituted, particularly by way of splitting of excitation bands and shifting of emission maximum to longer wavelengths.

To demonstrate the superiority of the phosphor obtained by G-C conversion over that of conventionally prepared phosphor, the well-known blue emitter $Ba_{1-x}Eu_xMgAl_{10}O_{17}$ ($0.1 < x < 0.4$) has been prepared by both the methods. The sample prepared by G-C conversion shows 10% higher quantum efficiency than the sample prepared by ceramic method.

### 3.2. *Luminescence of $Eu^{2+}$-doped nonstoichiometric barium orthoaluminate and their hydration reactions*

Large range of nonstoichiometry is observed in barium orthoaluminate with the general formula $Ba_{1-x}Al_2O_{4-x}$ ($0 < x < 0.56$) when prepared by the thermal decomposition of barium aluminium oxyhydroxide obtained by G-C conversion.[8] The large range of nonstoichiometry is

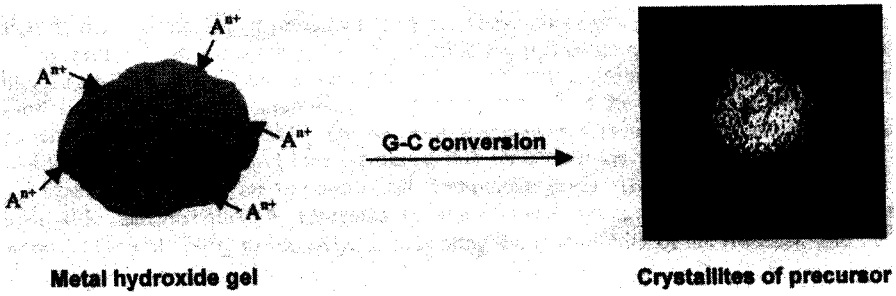

explained in terms of $Ba^{2+}$ vacancies within the corner sharing $AlO_4$ network, whereby 'nepheline' structure extends into 'stuffed' tridymite lattice. HREM studies indicated the ordering of point defects leading to the formation of extended defects and stacking faults. The coordination of $Al^{3+}$ remained tetrahedral as revealed by $^{27}Al$ MAS NMR. Barium orthoaluminate doped with $Eu^{2+}$ is a green-emitting phosphor with the emission maximum around 500 nm. As the $x$ value increases, the emission intensity also increases, although the position of the emission band remains the same. These phosphors are moisture sensitive and undergo hydration reaction.[9] On exposure to $CO_2$-free humid air, this compound reacted to form a new hydration product $Ba_{1-x}Al_2(OH)_{8-2x}.yH_2O$, wherein $Al^{3+}$ is in octahedral coordination. The collapse of the nepheline-type structure of barium orthoaluminate is explained in terms of the relative migration of $Ba^{2+}$ ions from the structural channels. Increase in the reaction rate for the nonstoichiometric samples is attributed to faster diffusion of the hydroxyl ions in the lattice, assisted by structural vacancies. The product is highly sensitive to $CO_2$; on exposure, this compound gives rise to barium aluminium carbonato oxyhydroxide and eventually segregates to $BaCO_3$ and aluminium hydroxide. Hydrated product decomposed around 600°C to $Ba_{1-x}Al_2O_{4-x}$ indicating the reversibility of the reaction. The $Eu^{2+}$ emission intensity of these nonstoichiometric phases reduced drastically on exposure to moisture and is completely quenched in the new hydration product.

### 3.3. *Synthesis and luminescence of $Eu^{2+}$- or $Ce^{3+}$-doped mullite and alkaline earth feldspars*

Mullite (2/1 and 3/2 mullite) is prepared by the decomposition of the hydrothermally synthesized precursor above 1300°C. $Eu^{2+}$ doped in 2/1-mullite shows emission around 420 nm, whereas that of 3/2 mullite is at 460 nm. The shift in the emission maximum of 3/2 mullite to the longer wavelengths is because of the increase in relative covalency as the $SiO_2$ content is larger than 2/1 mullite. The increase in covalency leads to large crystal field splitting, so that the energy difference between the ground and excited states is reduced, thereby shifting the emission to longer wavelengths. Different polymorphs of $MAl_2Si_2O_8$ ($M = Ca^{2+}$, $Sr^{2+}$, $Ba^{2+}$) and their solid solutions doped with $Ce^{3+}$ or $Eu^{2+}$ are prepared by G-C conversion by the reaction of hydrated alumina gel with $M(OH)_2$ ($M = Sr^{2+}$, $Ca^{2+}$, $Ba^{2+}$) and aerosol silica in the presence of aqueous ethanol at 80°C. The $Eu^{2+}$ and $Ce^{3+}$ luminescences show variation among the Ca-, Sr- and Ba-feldspars and their polymorphs. $Eu^{2+}$ doped in the hexagonal form of Ba- and Sr-feldspar shows two emission bands around 372, 442 and 372, 468 nm, respectively, whereas the monoclinic form of Sr-feldspar shows emission around 404 nm and those of Ba- and Ca-feldspars are at 436 nm and 420 nm, respectively. The interesting observation is the stabilization of $Eu^{2+}$ in $CaAl_2Si_2O_8$, $BaAl_2Si_2O_8$ (celsian) and their solid solution when fired in air along with some additives such as $B_2O_3$, MgO and $Li_2O$. This is because of the electron trapping by the $Eu^{3+}$ substituted at aliovalent $Ba^{2+}$ or $Ca^{2+}$ for the charge compensation reasons (i.e. $Eu^{3+} + e' \rightarrow Eu^{2+}$). $Ce^{3+}$ shows emission in the violet region in all the polymorphs exhibiting the characteristic double band emission (~342, 398 nm). However, the substitution of $B_2O_3$ suppresses the second emission band indicating that the aliocompositional substituents modify the crystal field at the $Ce^{3+}$ site. The phase relations in these systems are studied extensively.

### 3.4. *Photoluminescence of $Fe^{3+}$- or $Eu^{2+}$- or $Ce^{3+}$-doped $MAlSiO_4$ ($M = Na^+$, $K^+$)*

The polymorphs of $NaAlSiO_4$, namely, low-carnegieite, nepheline and high-carnegieite, are prepared by the decomposition of $NaAlSiO_4 \cdot 1.5H_2O$ (nepheline hydrate) obtained from G-C

conversion. Low-carnegieite is obtained by decomposing nepheline hydrate at 800°C, which has an orthorhombic structure and the X-ray diffraction pattern is indexed based on the space group Pmaa. Low-carnegieite is metastable and can be rehydrated to form nepheline hydrate. At 950°C, low-carnegieite transforms to nepheline which, in turn, transforms to high-carnegieite at 1300°C. Low-carnegieite and nepheline do not show any luminescence when doped with $Fe^{3+}$, whereas high-carnegieite exhibits deep red emission.[10] Non-emissivity of $Fe^{3+}$ is correlated to higher site symmetry in low-carnegieite and nepheline having $D_2$ and $C_{3v}$ symmetry, respectively, according to infrared spectral analysis. However, high-carnegieite has $C_{2v}$ site symmetry, due to rhombic distortion of tetrahedral sites during phase transformation that accompanies polyhedral rotation. Ferric ion-doped high-carnegieite shows strong emission band maximizing around 684 nm due to the $^4T_1(^4G) \rightarrow {}^6A_1(^6S)$ transition of $Fe^{3+}$ ($3d^5$). A weak emission arround 714 nm arises from the cooperative vibronic transition and another band around 674 nm emission is attributed to the $Fe^{3+}$ ion associated with the hole centre to form a defect complex of the type $Fe^{3+}$–$O^-$–$Si^{4+}$ as shown by EPR spectra. The presence of the defect centre in the vicinity of $Fe^{3+}$ changes the crystal field.

Unlike $Fe^{3+}$, rare-earth ions $Eu^{2+}$ and $Ce^{3+}$ show photoluminescence when doped in all the polymorphs. The emission characteristics are different among the polymorphs. $Eu^{2+}$-doped nepheline hydrate and low-carnegieite show emission in the blue region (460 and 468 nm, respectively), whereas nepheline and high-carnegieite show yellowish emission. The emission spectrum of nepheline and high-carnegieite unlike low carnegieite consists of multiple bands. The dominant peak is at 554 nm followed by 596 and 616 nm peaks. The multiple emission in nepheline and high-carnegieite is because of the occupation of $Eu^{2+}$ in different sites with different geometry; hence the site symmetry changes. Kalsilite, $KAlSiO_4$ doped with $Eu^{2+}$ shows a single emission band around 436 nm unlike the $NaAlSiO_4$ polymorphs, which emit at longer wavelengths. The $Ce^{3+}$ ion doped in these lattices does not show its characteristic doublet emission. A broad single emission band is observed. This is because of the strong crystal field at $Ce^{3+}$ site, which overcomes the splitting of the ground state due to spin-orbit coupling.

### 3.5. *Cationic distribution and its influence on the luminescence properties of $Fe^{3+}$-doped $LiAl_5O_8$ prepared by different wet chemical methods*

Cationic distribution during phase transition of synthetic mineral $LiAl_5O_8$ from the ordered primitive cubic to high-temperature spinel form is investigated using samples prepared by different routes, viz. gel to crystallite conversion, hydrothermal method, precipitation from excess sodium aluminate solution, and ceramic method.[11, 12] The solid-state magic angle spinning nuclear magnetic resonance spectra (MAS NMR) of $^7Li$ and $^{27}Al$ indicate that all the $Li^+$ ions are in octahedral sites and remain unaffected by the transformation, whereas the disorder involves the redistribution of $Al^{3+}$ ions in octa- and tetrahedral sites. Substitution of aliovalent ions such as $Zn^{2+}$ and $Mg^{2+}$ alters the t/o ratio. Ferric ion doped in ordered and disordered form of this compound shows deep red emission. Emission maximum of the ordered form is around 672 nm and that of disordered form has shifted to longer wavelengths, viz. 725 nm. Apart from this, a weak emission band is observed at 604 nm. The electron paramagnetic resonance spectra (EPR) indicate the presence of ($Fe^{3+}$–Vo)-defect complex, i.e. $Fe^{3+}$ ions associated with oxygen vacancies, in addition to the prevalence of $Fe^{3+}$ in both 4- and 6-coordinated sites having axial distortion. The luminescence spectra of $LiAl_5O_8$:$Fe^{3+}$ are explained in terms of defect-

related multiple centres involving ferric ions. The substitution of $Mg^{2+}$ shifts the emission maximum of the disordered form to shorter wavelengths (716 nm) and that of $Zn^{2+}$-substituted sample shows a long wavelength shift indicating that the modification in the cationic distribution also modifies $Fe^{3+}$ luminescence characteristics.

### 3.6. *Cation coordination and $Fe^{3+}$ luminescence in $LiAlO_2$ polymorphs prepared by hydrothermal method*

The polymorphs, $\alpha$-, $\beta$- and $\gamma$-$LiAlO_2$, were synthesized by a hydrothermal method. The as-prepared product obtained at 240°C was $\beta$-$LiAlO_2$, which converted completely to $\gamma$-$LiAlO_2$ above 1000°C. $\alpha$-$LiAlO_2$ was obtained by the decomposition of $LiAl(OH)_4$. $H_2O$ was prepared by the imbibition of Li(OH) into $LiAl_2(OH)_7.2H_2O$ hydrothermally at 140°C.[13] Solid-state MAS NMR studies indicate that $Li^+$ uniquely occupies octahedral sites in all the polymorphs. This observation indicates that the results of XRD and crystal structure studies on $\beta$ - and $\gamma$-$LiAlO_2$ reported in the literature that indicate the presence of $Li^+$ in the tetrahedral site are apparently in error with respect to $Li^+$ coordination. The other cation, $Al^{3+}$, occupied octahedral sites in $\alpha$-$LiAlO_2$ and tetrahedral sites in $\beta$- and $\gamma$-$LiAlO_2$. The $Fe^{3+}$ doped in various polymorphic forms of this compound was found to uniquely occupy octahedral $Li^+$ site. EPR spectrum of the $Fe^{3+}$ doped in these polymorphs indicates that this site is distorted during transformation. The $Fe^{3+}$ photoluminescent emission maximum was different for each polymorph ($\lambda_{em} = 712$, 724 and 732 nm, respectively, for $Fe^{3+}$ doped in $\alpha$-, $\beta$-, $\gamma$-$LiAlO_2$). The difference in the luminescence characteristics among the polymorphic forms is due to the change in site symmetry because of the distortion of the octahedra occupied by $Fe^{3+}$ across phase transition.

### 3.7. *Blue luminescence of $Fe^{3+}$-doped aluminium hydroxides and oxyhydroxides*

Blue luminescence is observed from the $Fe^{3+}$-doped Al-hydroxides and oxyhydroxides, namely, boehmite, pseudoboehmite, gibbsite or bayerite, which have only octahedral cation occupancy. The oxyhydroxides show more intense emission than the hydroxides. Emission spectrum consists of three broad bands peaking at 400, 420 and 468 nm. The corresponding excitation bands are observed at 345, 356 and 376 nm. The blue emission is not due to the d-d transition of octahedral/tetrahedral $Fe^{3+}$ ion as the excitation spectrum does not show sharp absorption bands due to $^6A_1(^6S) \rightarrow {}^4E, {}^4A_1(^4G)$ transition, a feature specific to $Fe^{3+}$ internal transition. The blue emission is assigned to $Fe^{3+}$–$V_o$ defects complex based on EPR investigations. The $Fe^{3+}$ ion in the 6-coordinated site with an axial distortion associated with a point defect such as oxygen vacancy forms a defect complex, $Fe^{3+}$–Vo, which gives rise to dominant signal at g = 4.270 and the other very weak signal is due to the oxovanadyl ($VO^{2+}$) cation. The $VO^{2+}$ center in this host quenches luminescence of $Fe^{3+}$–$V_o$ defect center.

## References


1. BUTLER, K. H. — *Fluorescent lamp. Phosphors*, The Pennsylvania State University Press, University Park, 1981.
2. ELENBASS, W. (ED.) — *Fluorescent lamps*, Macmillan, 1971.
3. BLASSE, G. AND GRABMAIER, G. — *Luminescent materials*, Springer-Verlag, 1994.
4. BLASSE, G. — *Prog. Solid St. Chem.*, 1988, **18**, 79.

5. JENKINS, H. G., MCKEAG, A. H. AND RANBY, P. H. — *J. Electrochem. Soc.*, 1949, **96**, 1.
6. STEVELS, A. L. N. AND SCHRAMA-DE PAUW, A. D. M. — *J. Electrochem. Soc.*, 1976, **123**, 691.
7. KUTTY, T. R. N. AND NAYAK, M. — *Mat. Res. Bull.*, 1995, **30**, 325.
8. NAYAK, M. AND KUTTY, T. R. N. — *Mat. Res. Bull.*, 1996, **31**, 227.
9. KUTTY, T. R. N. AND NAYAK, M. — *Cem. Concr. Res.*, 1998, **28**, 1393.
10. NAYAK, M. AND KUTTY, T. R. N. — *Mat. Chem. Phys.*, 1998, **57**, 138.
11. NAYAK, M., KUTTY, T. R. N., JAYARAMAN, V. AND PERIASWAMY, G. — *J. Mat. Chem.*, 1997, **7**, 2131.
12. KUTTY, T. R. N. AND NAYAK, M. — *J. Alloys Compounds*, 1998, **269**, 75.
13. KUTTY, T. R. N. AND NAYAK, M. — *Mat. Res. Bull.*, 1999, **34**, 249.


Thesis Abstract (Ph. D.)

**Structural studies of biologically active and conformationally important oligopeptides: Implications for *de novo* design** by Ravindranath Singh Rathore
Research supervisor: Prof. N. Shamala
Department: Physics

## 1. Introduction

The central goal in designing a novel protein or peptide structure is to devise an amino acid sequence that will adopt a unique and stable 3-dimensional structure. Although nature has provided an enormous number of natural proteins, which fold into different variety of structures and carry out innumerable functions, there are two main motivations to pursue the protein and peptide design: (i) it is the ultimate test of our understanding of natural proteins, and (ii) it represents an essential first step towards a new generation of novel structures that will have practical applications in industry and biomedicine. Among the several approaches that have been tried the one that emerged successful is the *de novo* design—the design of peptides and proteins from a scratch. Here the problem is addressed in steps, i.e. first build modules of secondary and super secondary structures and then assemble them into 3-D structures of desired conformation and function. The available tools to design are not just limited to conventional 20 genetically coded amino acids but comprise various mutated, constrained or restrained flexible amino acids or even templates.[2,3] In our work, we have made an attempt to evaluate the suitability of constrained and other nonstandard amino acids for the design of biologically and conformationally important peptides, in the *de novo* design approach.

## 2. Experimental procedures

Results were obtained using single-crystal X-ray crystallographic and computational (molecular dynamics) techniques. Synthesis, solution and chemotactic activity studies of peptides were

carried out elsewhere as part of a collaborative work. Diffraction studies: intensity data were collected on Enraf-Nonius CAD-4 and Rigaku MSC/AFC 7s diffractometers. Structures were solved by the application of direct and Patterson methods, and refined by full-matrix least-square methods.[4] Simulation studies: molecules were simulated for 540 picoseconds (40 ps for equilibration + 500 ps for data collection), using consistent valence force field (CVFF),[5] after minimization of refined crystal structure coordinates.

## 3. Results and discussion

Three chemotactic *N*-formyl peptides, which induce chemotaxis and lysozyme enzyme release, were studied to assess their conformation–activity relationship, in view of the current model on structure–function relationship, which suggests two widely different conformations–folded and extended–to be biologically active.[6] The following peptides were investigated:

*N*-formyl-L-methionyl-1-amino 1-cyclooctane carbonyl ($Ac_8c$)-L-phenylalanyl-methyl ester (fMACF); *N*-formyl-L-methionyl-dipropylglycyl-L-phenylalanyl–methyl ester (fMDF), and *N*-formyl-L-methionyl-L-leucyl-L-*paraiodo* phenylalanyl–OH (fMLIF), using local cyclic and linear constraints, or modifications, at positions 2 and 3 of prototypic peptide *N*-formyl-met-leu-phe-OMe (fMLF). Conformational studies of peptides indicate that fMACF and fMLIF have folded conformation, while fMDF assumes extended backbone conformation, both in crystalline state and solution. Peptides in these conformations demonstrate significant chemotactic and secretagogue (lysozyme secretion) activities.[7] The present study demonstrates efficacy of nonstandard amino acids to lock the peptide conformation in its biologically active state. The high biological activity of peptides with widely different conformations may possibly be explained on the basis of *induced-fit* theory, i.e. there is a possible change in the conformation of peptides on receptor binding. The molecular dynamics study performed on fMDF with a view to observe other conformations accessible to peptide does indeed demonstrate that folded conformation is accessible to the molecule at room temperature. It can be inferred that receptor would induce single conformation of peptide by minimizing the total energy of peptide–receptor complex.

Few peptides from linearly and cyclic disubstituted glycine were examined, to address such issues as conformational variability, sequence-dependent conformational preferences, design and stereochemistry of linker segments, show interesting features. Boc-Aib-$Ac_8c$-Aib-OMe is one such peptide, which incorporates 1-amino 1-cyclooctane carboxylic acid ($Ac_8c$). It forms type-III(III′)$\beta$-turns in the crystal. Examining the conformational preference of Aib-Xaa-Aib sequence reveals that similar to homo-oligomeric sequence of Aib, it also has a strong tendency to make type-I or –III $\beta$-turn. Another molecule, Boc-L-Val-Aib-L-Leu-OMe, which has achiral sequence Aib-Gly at the middle that has strong tendency to make $\beta$-turn, adopts consecutive type II–I′ $\beta$-turn conformation. Examining the collective behaviour from crystal structure analysis of these $C^{\alpha,\alpha}$ disubstituted glycine, reported in literature,[8,9] reveals that 1-aminocycooctane carboxylic acid, $Ac_8c$, exhibits conformational preferences comparable to Aib. In case of linearly disubstituted glycine, conformational preferences of higher homologs of Aib are at variance due to marginal differences between lowest-energy fully extended and helical conformations:[3] in small peptides they adopt helical and fully extended conformations with equal preference, while in long sequences they invariably prefer helical conformation.

Cyclooctane ring, present in $Ac_8c$ residues, assumes lowest energy *Boat–Chair* conformation with $C^{\alpha}$ atom at the basal position in the boat segment. *Quasi*-equatorial and -axial positions are occupied by amino and carbonyl groups. The asymmetry parameters of BC conformation are close to zero, indicating that they are not significantly distorted from ideal boat-chair conformation.

As opposed to constrained residues, $\omega$-amino acids[10] are another important molecular tools, which relish a high degree of flexibility, and are useful for generating several new kinds of sheets, turns or helices. Structure of Boc-$\beta$-Ala-L-Leu-Aib-L-Val-OMe has been reported. The sequence adopts an open $\beta$-turn conformation in solid state.

Limited success, however, was achieved with constrained residues, as they restrict the peptide backbone only in the helical region of conformational space (Ramachandran map). Extended structures, such as $\beta$-sheets, remain largely unexplored in the absence of any suitable candidate, which compulsorily gives rise to $\beta$-sheet structures.[2] They are poorly packed in a crystal tending to aggregate and therefore do not exist in isolation; this has limited their study in solid or solution state. We attempted to analyse those peptides which form $\beta$-sheets in crystals. With solid-state studies on one of the peptides, Z-L-Ala-L-Ala-L-Leu-pNA, four different conformers of which aggregate to form infinite anti-parallel $\beta$-sheet, it was found that non-covalent $\pi$ (aromatic)-interactions such as $\pi \ldots \pi$ and $\sigma \ldots \pi$ interactions, can play a very important role in stabilizing the packing of sheets in crystal. The high flexibility of peptide, as evidenced from four different conformers co-crystallized in an asymmetric unit, is also demonstrated in molecular dynamics study.

## 4. Appendix

In conjunction with these studies, crystal structures of two peptide hydrates: L-tryptophylglycine monohydrate; and glycyl-L-glutamine monohydrate were also examined. Crystal structure analysis highlights water-mediated peptide linkage. Apart from formation of several three-center motifs, one of the interesting features observed is that water molecules aggregate to form channels in the crystal.

## References


1. HECHT, M. H. — In *Protein engineering and design* (P. R. Carey, ed.), Academic Press, 1996, pp. 1–50.
2. BALARAM, P. — *Curr. Opin. Struct. Biol.*, 1992, **2**, 845–851.
3. BENEDETTI, E. AND TONIOLO, C. — In *Polymeric materials encyclopedia*, Vol. 8 (J. C. Salamone, ed.), CRC Press, 1996, pp. 6472–6481.
4. SHELDRICK, G. M. — *SHELX 97: Program for the solution and refinement of crystal structures*, Univ. of Göttingen, Germany, http://shelx.uni-ac.gwdg.de/SHELX/
5. — *Discover: Package for molecular simulation, Version 2.9.5*, Biosym Technologies Inc., San Diego, USA, http://www.biosym.com/solutions/products/insight/

6. BECKER, E. L., FREER, R. J., TONIOLO, C. AND BALARAM, P. — In *Membrane receptors and cellular regulation* (M. P. Czech and C. R. Kahn, eds.), 1985, pp. 129–134, A. R. Liss, NY, USA.

7. PRASAD, S. *et al.* — *Int. J. Peptide Protein Res.*, 1996, **48**, 312–318.

8. MORETTO, V. *et al.* — *J. Peptide Sci.*, 1996, **2**, 14–27.

9. DATTA, S. — *Folding of designed peptides: X-ray crystallographic studies on the structure, conformation, aggregation and interactions of oligopeptides containing conformationally constrained amino acids*, Ph. D. Thesis, Indian Institute of Science, Bangalore, 1998.

10. BANERJEE, A. AND BALARAM, P. — *Curr. Sci.*, 1997, **73**, 1067–1077.


Thesis Abstract (Ph. D.)

**Quasicrystals, rational approximants and quasicrystalline tilt boundaries: Theory and experiments** by K. Ramakrishnan

Research supervisors: Profs S. Ranganathan and T. V. Ramakrishnan

Department: Physics

## 1. Introduction

In 1974, Roger Penrose showed that an aperiodic tiling of planar surfaces with fivefold rotational symmetry can be achieved by using only two different kinds of tiles. In 1984, this theoretical interest turned into a technologically relevant pursuit, when Dan Shechtman discovered quasicrystals, an ordered solid with a non-crystallographic symmetry. Since then quasiperiodicity is known to occur in various dimensions. The icosahedral quasicrystal (space group Pm $\bar{3}\bar{5}$) is three dimensional, while the decagonal quasicrystal (space group $P10_5/mcm$) is two dimensional. For a geometrical discussion of tiling, see Lord *et al.*[1]

## 2. An algorithm for the projection method for arbitrary dimensions

With increasing experimental sophistication, data on quasicrystalline phases have become more accurate and there is a need to develop computable theoretical tools. An algorithm to project $N$-dimensional unit hypercube in $\boldsymbol{E}$ to $n$-dimensional subspace ($\boldsymbol{E}_{\parallel}$) was devised and the algorithm has been implemented as a computer program written in C-language. The algorithm needs a matrix $\boldsymbol{R}(N \times N)$, $N$ and $m$ (dimensionality of $\boldsymbol{E}_{\perp}$ subspace). $\boldsymbol{R}(N \times N)$ can be divided into two matrices $\boldsymbol{A}(n \times N)$ and $\boldsymbol{B}(m \times N)$. First, a window $\boldsymbol{W}$ is generated in $\boldsymbol{E}_{\perp}$ subspace using $\boldsymbol{B}(m \times N)$, where $m + n = N$. Points in $\boldsymbol{E}$, which fall inside the window $\boldsymbol{W}$ in $\boldsymbol{E}_{\perp}$, by using $\boldsymbol{B}(m \times N)$, are then projected on to the $\boldsymbol{E}_{\parallel}$ subspace using $\boldsymbol{A}(n \times N)$. The set of projected points in $\mathbf{E}_{\parallel}$ subspace is the required quasiperiodic structure, which is the output of the algorithm. For the calculation of the window $\boldsymbol{W}$, a unit hypercube of dimension $N$ is generated by an orthogonal $N \times N$ matrix $\boldsymbol{R}$. That is, the coordinates of the lattice points are all the linear combinations of the columns of $\boldsymbol{R}$ with integer coefficients $(x^1, x^2, x^3, \ldots, x^N)$.

We have a generalized lattice in $\boldsymbol{E}_{\perp}$ given by linear integer combinations of the columns of $\boldsymbol{B}$:

$$\boldsymbol{b}_1 x^1 + \boldsymbol{b}_2 x^2 + \boldsymbol{b}_3 x^3 + \boldsymbol{b}_4 x^4 + \cdots + \boldsymbol{b}_N x^N. \quad (1)$$

The $2^N$ vertices of a single $N$-dimensional hypercube $\gamma_N$, of unit edge-length, centred at the origin, project to the $2^N$ points in $E_\perp$.

Each $(m-1)$-dimensional facet of $\gamma_N$ is determined by $m$ of the points (1). There are $2^{N-m+1}\binom{N}{m-1}$ such facets. Each $(m-1)$-facet contains $2^m$ vertices of $\gamma_N$. Each $(m-1)$-facet belongs to a set of $2^{N-m+1}$ parallel facets. They project, in general, to sets of parallel hyperplanes in $E_\perp$. Let

$$\boldsymbol{n} \cdot \boldsymbol{x} = d_i \ (i = 1, 2, \ldots, 2^{N-m}) \tag{2}$$

be the equations, in $E_\perp$, of the hyperplanes of such a set. $\boldsymbol{n}$ is the unit normal to the hyperplane, as the $|d_i|$ are their distances from the origin. If $d = \max_{\|} |d_i|$, then $\boldsymbol{n} \cdot \boldsymbol{x} = \pm d$ are two bounding hyperplanes of the window. It is preferred to write the equation (II.3) in the form $\pm \boldsymbol{q}_i \cdot \boldsymbol{x} = 1$. The two boundary hyperplanes are then $\pm \boldsymbol{q} \cdot \boldsymbol{x} = 1$, where $q$ is the $\boldsymbol{q}_i$ with the least length. The window region is then determined by the set of inequalities.

$$-1 < \boldsymbol{q} \cdot (\boldsymbol{x} + \boldsymbol{y}) \leq 1 \tag{3}$$

($\boldsymbol{y}$ is an optional shift of origin), for the vectors $\boldsymbol{q}$ obtained from all the $\binom{N}{m-1}$ sets of parallel hyperplanes. A mention must be made of a new numerical technique used to solve the linear equations in the algorithm, which can solve under/over determined linear equations. This allows the algorithm to be used in cases when $N \cdot m + n$, shown in the case of dodecagonal symmetry. Since the output is the coordinates (in $n$-dimensions) of the vertices in the quasiperiodic tilings, another program/software is needed for visualization in 2D and 3D. A methodology using the available software to visualize the results has also been implemented.[2] It is now possible to visualize the result of the algorithm in a VRML (virtual reality markup language) viewer for $n = 3$.

### 3. Rational approximant structures to icosahedral and decagonal quasicrystals

The rational approximants were investigated. In the literature,[3] there are some phases which have been wrongly identified as rational approximants to both icosahedral and decagonal quasicrystals. The Little phase, an orthorhombic (pseudotetragonal) ($a = 2.51$ nm; $b = 2.24$ nm; $c = 3.03$ nm) crystalline phase, was wrongly considered to be an approximant to decagonal quasicrystal. The Little phase occurs in many alloy systems – Al–Cr, Al–Mn–Zn, Al–Mn–Cr–Si, Al–Mn–Ni[4] and Al–Fe–Cr. It has been proved in this study that the Little phase is an icosahedral approximant by a study of the transformation routes from quasicrystalline to crystalline phases and by comparing the reflections from electron diffraction patterns, XRD results and theoretical calculations. A stereographic analysis of the Little phase showed a strong resemblance to the icosahedral quasicrystal.

The orthorhombic approximant phases to the decagonal quasicrystal occur in many alloy systems. The various orthorhombic approximants have been classified into two types—the Robinson type and the Taylor type. The decagonal quasicrystal has been described by a twinning of the icosahedral quasicrystal about the $[1\tau 0]$ axis. It is shown that the Taylor and the Robinson approximants can be described as a twinning of the Mackay cubic approximant and the Little orthorhombic approximant to the icosahedral quasicrystal, respectively.

A new structural model for the identification of hexagonal derivatives has been discovered. There exist several approximants to the icosahedral, the decagonal and the hexagonal quasicrystals. Earlier, some of these have been identified as approximants to a particular quasicrystal, e.g. the hexagonal $\mu$-$Al_4Mn$ was identified as a decagonal approximant. In this study, a scheme has been devised based on a structural unit in which three icosahedra are arranged with their twofold axis common and the adjacent icosahedra twinned across the fivefold axis. This scheme explains correctly the mutually perpendicular sixfold, pseudo tenfold and twofold axes seen in the hexagonal quasicrystal and various other crystalline (hexagonal, orthorhombic and monoclinic) phases, which therefore are identified as hexagonal derivatives.

## 4. Experimental studies on Al–Mn–Zn alloys

An experimental investigation to study crystalline and quasicrystalline phases in Al–Mn–Zn alloys was done.[5] Three Al–Mn–Zn alloys and one Al–Mn–Zn–Si alloy were melted. These alloys were melt-spun on single rotating Cu wheel. As-cast alloys showed approximant phases embedded in the Al matrix and the melt-spun alloys showed quasicrystalline phases. The melt-spun alloys were extremely brittle. These alloys were studied using optical microscopy, SEM and TEM. The quasicrystalline and rational approximant structure phases were found in the as-cast and melt-spun alloys.

The 7075 alloy is an age-hardenable Al–Zn–Mg-based alloy. It has an excellent combination of low density and high strength, making it very suitable for the transportation industry. Two of the above alloys were mixed with 7075 alloy to produce a new 'quasicrystal composite'. The hard quasicrystalline phase is embedded in the soft Al matrix. As expected, the as-cast composites show crystalline and quasicrystalline phases embedded in the Al matrix. The melt-spun alloys show Al and quasicrystalline phases.

## 5. Quasiperiodic crystalline tilt boundaries

Grain boundaries are divided into two classes – special and random boundaries.[6] Special boundaries have low values of $\Sigma$, the reciprocal of the density of coinciding points in the coincidence site lattice (CSL). All values of $\Sigma$, for a given misorientation $\theta$ about a specific axis of misorientation $[UVW]$, can be calculated (for cubic crystals) using the formulae:

$$\Sigma = x^2 + N y^2, \tag{4}$$

$$\tan(\theta/2) = y\sqrt{N}/x, \tag{5}$$

where $N = U^2 + V^2 + W^2$ and $x$ and $y$ are integers $\geq 0$.

Large-angle (>10°) tilt boundaries can be described by the CSL model. $\Sigma$ is directly related to the angle of tilt. $\Sigma = \infty$ implies no coincidence, which in turn implies quasiperiodicity. According to SUM (structural unit model), $\Sigma = \infty$ boundaries can be approximated by two lower $\Sigma$ boundaries. Five different $\Sigma = \infty$ boundaries in several quasicrystalline symmetries were considered. They are $\Sigma = \infty[100]45°$, $\Sigma = \infty[100]30°$, $\Sigma = \infty[110]90°$, $\Sigma = \infty[111]30°$ and $\Sigma = \infty[111]44.48°$. For each of these boundaries, two lower $\Sigma$ boundaries were found. The lower $\Sigma$ boundaries are arranged quasiperiodically to match the corresponding $\Sigma = \infty$ boundary. Each of these $\Sigma = \infty$ boundaries have an infinite series associated with them like $\Sigma = \infty[110]90°$ boundary having the octanacci series (recursion relationship $F_{n+1} = 2F_n + F_{n-1}$).

The relationship between CSL and QPSL (quasiperiodic superlattice) has also been explored. Orientation of the window ($W$) and the projection hyperplane ($E_{\parallel}$) gives rise to different structures. Quasiperiodic superlattices (QPSL) are generated when the orientation of the projection plane ($E_{\parallel}$) is irrational and that of the strip ($W$) is irrational. In particular, the dodecagonal quasiperiodic superlattice and $\Sigma = 7$ CSL are shown to be related to one another.

## References


1. LORD, E. A., SEN, S. K. AND VENKAIAH, V. CH. — *Simulation*, 1990, **54**, 239; *Neural Parallel Sci. Computations*, 1996, **4**, 325.
2. SENECHAL, M. — *Quasicrystals and geometry*, Cambridge University Press, 1995.
3. ELSER, V. AND HENLEY, H. L. — *Phys. Rev. Lett.*, 1985, **55**, 2883.
4. SINGH, A. AND RANGANATHAN, S. — *Mater. Sci. Engng A*, 1994, **181/182**, 754.
5. RANGANATHAN, S. AND CHATTOPADHYAY, K. — *A. Rev. Mater. Sci.*, 1991, **21**, 437.


Thesis Abstract (Ph. D.)

**Folding of the designed peptides: X-ray crystallographic studies on the structure, conformation, aggregation and interactions of oligopeptides containing conformationally constrained amino acids** by Saumen Datta
Research supervisor: Prof. N. Shamala
Department: Physics

## 1. Introduction

Understanding the relations between amino acid sequences and protein structures and functions are one of the important problems of modern molecular biology. But this is a daunting prospect because of the complexity of protein structures. Polypeptide sequences consisting of the 20 genetically coded amino acids possess structural flexibility which makes the predictions difficult.[1] However, nonprotein amino acids modified at $C^{\alpha}$ carbon atoms have novel structural property of restricting the available conformational space and could be used as stereochemical directors of polypeptide folding. The use of such conformationally rigid residues could permit the construction of structurally well-defined molecules like helices and strands which can then be assembled by flexible linker peptides into super secondary structural motifs which can mimic proteins.[2,3] Thus the study of synthetic polypeptides mimicking the folding patterns of proteins is a subject of intense current research.

Crystal structure determination of oligopeptides provides an opportunity to characterize specific conformational states in flexible molecules. Comparison of the solid-state conformations of the same sequence segments determined under different conditions can provide information on the conformational excursions that are possible. Investigations of synthetic peptides containing amino acid residues with contrasting conformational tendencies afford a means of evaluating the role of sequence and environmental effects. The crystal structure determinations

often yield surprising results providing unanticipated insights into the conformations, modes of aggregation, hydrogen bond interactions and solvation of the peptides.[4,5] Some examples of all these based on the investigations carried out on 12 peptides containing conformationally constrained amino acids form the theme of this work.

The work reports results of X-ray crystallographic studies of 12 oligopeptides listed below. Within brackets are given the abbreviations used for the sequences.

1. Boc-Ala-Ile-Aib-OMe (AIU)
2. Boc-Aib-Ala-Ile-Aib-OMe (U14)
3. Boc-Gly-Gly-Leu-Aib-Val-OMe (GV5)
4. Boc-Val-Ala-Leu-Aib-Val-Ala-Leu-OMe (VF7)
5. Boc-Pro-Aib-Gly-Leu-Aib-Leu-OMe (RH2)
6. Boc-Leu-Aib-Val-Ala-Leu-Aib-Val-OMe (LAV7)
7. Boc-Leu-Aib-Val-Gly-Leu-Aib-Val-OMe (LGV7)
8. Boc-Leu-Aib-Val-Ala-Leu-Aib-Val-Ala-Leu-Aib-OMe (LAL10)
9. Boc-Leu-$Ac_8$c-Ala-Leu-$Ac_8$c-OMe (LAC5)
10. Boc-Leu-$Ac_8$c-Ala-Leu-$Ac_8$c-Ala-Leu-$Ac_8$c-OMe (LAC8)
11. Boc-Gly-Dpg-Gly-OH (GDG)
12. Boc-Val-Val-Ala-Leu-Gly-Dpg-Gly-Val-Ala-Leu-Aib-Val-Ala-Leu-OMe (GDG14)

## 2. Methods

All the peptides were synthesized at Prof. P. Balaram's laboratory at the Molecular Biophysics Unit, Indian Institute of Science, Bangalore. All the crystals were grown by slow evaporation methods from methanol/water. A single crystal of each was used in four-circle diffractometer for three-dimensional diffraction intensity collection. Structures were solved either by direct phase determination methods or combination of vector search methods and partial structure expansion methods. Structures were refined at first isotropically and then anisotropically. Hydrogen atoms were not identified from the electron density maps, but fixed geometrically with all the nonhydrogen atoms after anisotropic refinement.

## 3. Results and discussion

The diastereomeric mixture of the tripeptide, Boc-Ala-Ile-Aib-OMe, crystallizes in the triclinic space group P1, with four molecules in the asymmetric unit. It provides an example of serendipitous observation of both parallel and antiparallel $\beta$-sheet hydrogen bonding patterns in the same crystal.[6] Whereas the overwhelming majority of examples reported so far associate in an antiparallel fashion, this structure provides a novel example of coexistence of both parallel and antiparallel modes of aggregation in the same crystal form. Interestingly, Aib residue does not form part of the observed $\beta$-sheet and indeed adopts the expected helical ($\phi$, $\psi$) values. Extension of the tripeptide segment by the addition of a residue at the N-terminus in Boc-Aib-Ala-Ile-Aib-OMe resulted in a $3_{10}$-helical conformation with two consecutive type-III $\beta$-turns.

Dramatically different conformations for the Gly-Gly-Leu-Aib-Val segments have been observed in the crystal structure of the pentapeptide, Boc-Gly-Gly-Leu-Aib-Val-OMe and a

protected octapeptide Boc-Gly-Gly-Leu-Aib-Val-OMe reported.[7] Octapeptide takes helical conformation in crystals with Gly-Gly segment comfortably accommodated at the center of the helix. In sharp contrast, in the pentapeptide Leu-Aib segment forms type-II $\beta$-turn ($\phi_3 = -61°$, $\psi_3 = 130°$, $\phi_4 = 71°$, $\psi_4 = 6°$) with the Gly-Gly arm adopting an extended conformation ($\phi_1 = -92°$, $\psi_1 = 133°$, $\phi_2 = 140°$, $\psi_2 = 170°$).

The heptapeptide, Boc-Val-Ala-Leu-Aib-Val-Ala-Leu-OMe, has crystallized in $P2_1$ space group with two molecules in the asymmetric unit. The analysis of the conformations of the two independent peptide helices in the crystallographic asymmetric unit of this heptapeptide provides an opportunity to emphasize the observation of C-terminus distortion in helices and to present an analysis of 4→1/5→1 hydrogen bonding patterns in peptide helices. Both molecules in the asymmetric unit adopt helical conformations with ($\phi$, $\psi$) values for residues 1 to 6 in the right-handed helical region. Large deviations from ideal helical ($\phi$, $\psi$) values are observed at Val(5) and Ala(6) in both molecules with distortions being more pronounced in the latter case. Significant differences are observed at Phe(7) which may be indicative of a greater tendency of short peptide helices to fray at the C-terminus. The helix type in the molecule is determined by analyzing both 4→1 and 5→1 hydrogen bond interactions and comparison with the result of an analysis of protein structures. Indeed, the presence of two 4→1 hydrogen bond interactions, in addition to four 5→1 interactions in both the conformations provides an opportunity to characterize bifurcated hydrogen bonds.

Crystal structures of a hexapeptide Boc-Pro-Aib-Gly-Leu-Aib-Leu-OMe and the two heptapeptides Boc-Leu-Aib-Val-Ala-Leu-Aib-Val-OMe, Boc-Leu-Aib-Val-Gly-Leu-Aib-Val-OMe adopt right-handed helical conformations terminated by a structural motif widely known as Schellman motif.[8] The Schellman motif is a widely observed, helix terminating structural motif in proteins[9, 10] which is achieved by the addition of a left-handed helical ($\alpha_L$) conformation by a C-terminus residue. The resulting hydrogen bonding pattern involves an intramolecular 6→1 interaction and concomitant formation of a 5→2 interaction. This helix-terminating motif is readily mimicked in synthetic helical peptides by placing an achiral residue at the penultimate position of the helix.[11] Crystal structure of both the heptapeptide reveals a $3_{10}$-helix terminated by a Schellman motif with Aib(6) adopting an $\alpha_L$ conformation. In both the cases, a 6→1 hydrogen bond between Aib(2)CO...Leu(7)NH and a 5→2 hydrogen bond between Val(3)CO...Aib(6)NH are observed. The structure of the hexapeptide $RH_2$, related to the C-terminal segment of the peptide antibiotic efrapeptin, in crystals reveals a short helical stretch terminated by a Schellman motif. The structure also reveals an interesting hydration pattern which is of relevance in the context of a recent discussion on the role of hydrated peptide backbone in the folding process.[12]

The crystal structure of the decapeptide, Boc-Leu-Aib-Val-Ala-Leu-Aib-Val-Ala-Leu-Aib-OMe, reveals a perfect $\alpha$-helix. From the analysis of the oligopeptides, it was observed that when Aib is placed at the penultimate position of a sequence, conformations of the sequences are invariably terminated with the formation of a Schellman motif at the C-terminus.[11] The achiral nature of the Aib residue favors the helix reversal by adopting the $\alpha_L$ conformation and thus facilitates the termination with the formation of a 6→1 hydrogen bond. The question that emerged from these studies, obviously, was what would happen to such helices when more residues are added at the C-terminus. Accordingly, two decapeptide sequences Boc-Leu-Aib-

Val-Ala-Leu-Aib-Val-D(Ala-Leu)-Aib-OMe (LAD10) and Boc-Leu-Aib-Val-Ala-Leu-Aib-Val-Ala-Leu-Aib-OMe (LAL10, a control peptide) which are the extension of Boc-Leu-Aib-Val-Ala-Leu-Aib-Val-Ala-Leu-Aib-OME (LAL10, a control peptide) which are the extension of Boc-Leu-Aib-Val-Ala-Leu-Aib-Val (LAV7) by the addition of three D residues and three L residues were synthesized and crystallized. The crystals of LAD10 were very fragile and also very small to give good diffraction data. In contrast good, stable crystals were obtained with LAL10 and X-ray diffraction studies were completed. It is noteworthy that whereas the heptapeptide LAV7 adopts $3_{10}$-helical conformation terminated with the formation of a Schellman motif, the decapeptide LAL10 which is obtained by adding three more L-residues to LAV7 form a continuous α-helix.

$C^{\alpha,\alpha}$-dialkylated amino acid residues, containing both linear and cycloalkane sidechains also have been shown to strongly stabilize helical conformations. Thus far, only relatively short peptides containing 1-aminocycloalkane-1-carboxylic acids ($Ac_nc$) have been structurally characterized for ring sizes ($n$) ranging from 3 to 12 membered rings. The sequences, Boc-Leu-$Ac_8c$-Ala-Leu-$Ac_8c$-OMe (LAC5), Boc-Leu-$Ac_8c$-Ala-Leu-$Ac_8c$-Ala-Leu-$Ac_8c$-OMe (LAC8), studied are chosen to place the cyclooctane ring approximately on the same face of approximately cylindrical $3_{10}/\alpha$-helical structures. While LAC5 folds into a short segment of $3_{10}$-helix, LAC8 adopts a mixed $3_{10}/\alpha$-helical fold with insertion of a water molecule into the peptide backbone. The crystal structures also provide conformational characterization of five independent cyclooctane rings, four of which adopt classical boat–chair conformations, while the fifth is appreciably distorted, resembling a chiral intermediate in the pseudorotational pathway from the boat-chair to the twisted boat–chair conformations.[13]

The ability to construct stereochemically well-defined peptide helices, using α-aminoisobutyric acid (aib) and related $\alpha,^8$-dialkylated glycines,[14] stimulated attempts to assemble helix-linker-helix motifs as models for supersecondary structures in proteins.[2] The use of nonhelical linker should facilitate design of molecules with distinct helical segments. Closed pack, approximately antiparallel helix arrangement may then be achieved as a consequence of large complementary molecular surfaces. Structural investigation of Gly-Dpg-Gly segment in peptide sequences is a search for a proper linking segment between two helices. Crystal structures of a tripeptide Boc-Gly-Dpg-Gly-OH (GDG) and a 14 residue peptide Boc-Val-Val-Ala-Leu-Gly-Dpg-Gly-Val-Ala-Leu-Aib-Val-Ala-Leu-OMe (GDG14) were solved as a part of this investigation. The use of Gly-Dpg-Gly, in the present study, was dictated by the fact that Gly is highly conformationally flexible and has a relatively low helix propensity. While the Dpg residue adopts a fully extended conformation in the tripeptide (GDG), a continuous helix is obtained in the 14 residue peptide (GDG14). The GDG14 molecule forms an almost $\alpha$-helical structure, stabilized by successive 5→1 hydrogen bonds. As frequently observed in peptide helices there is a $3_{10}$-helical turn at the N-terminus with a 4→1 hydrogen bond between the Boc(0)CO and Ala(3)NH groups. A single $3_{10}$-helical hydrogen bond is also observed near the C-terminus between Leu(10)CO and Ala(13)NH groups. In the center of the helix there is evidence for a possible transition between $\alpha$ and $3_{10}$-helical structures. Gly(5)CO appears to be involved in a 4→1 interaction with Val(8)NH, while a corresponding 5→1 interaction with Ala(9)NH is definitely weaker as indicated by the N...O distances. In crystal packing of GDG14, a lone methanol molecule is trapped between helical columns and forms a single hydrogen bond with the CO group of Ala(3). This is a relatively rare example of solvation involv-

ing bifurcated hydrogen bond formation to a CO group involved in a strong intrahelical hydrogen bond. Comparison with other crystallographically determined Gly-Dpg-Gly segments reveals a significant degree of conformational variability in the sequence.

## 4. Conclusions

Although the results obtained so far have demonstrated that the design of synthetic peptides with desired structures is indeed a feasible enterprise, further studies on longer peptides and even modifications on the functional groups of sidechain would doubtless reveal some surprises. The subtle conformational effects of substituents could make a strong contribution to our understanding of protein folding. The most reliable and specific new information will be obtained only after several cycles of design, structure determination and redesign.

## References


1. HECHT, M. H., RICHARDSON, J. S., RICHARDSON, D. C AND OGDEN, R. C. — *Science*, 1990, **243**, 622–628.
2. BALARAM, P. — *Curr. Opin. Struct. Biol.*, 1992, **2**, 845–851.
3. KARLE, I. L. *et al.* — *J. Am. Chem. Soc.*, 1995, **117**, 9632–9637.
4. KARLE, I. L., BANERJEE, A., BHATTACHARYYA, S. AND BALARAM, P. — *Biopolymers*, 1996, **38**, 515–526.
5. KARLE, I. L. — *Acta Crystallogr. B*, 1992, **48**, 341–356.
6. DATTA, S., SHAMALA, N., BANERJEE, A. AND BALARAM, P. — *Int. J. Peptide Protein Res.*, 1996, **48**, 209–214.
7. KARLE, I. L. — *Biopolymers (Peptide Sci.)*, 1996, **40**, 157–180.
8. SCHELLMAN, C. — *Protein folding* (Jaenicke, R., ed.), Elsevier/North-Holland Biochemical Press, 1980, pp. 53–61.
9. AURORA, R., SRINIVASAN, R. AND ROSE, G. D. — *Science*, 1994, **264**, 1126–1130.
10. NAGARAJARAM, H. A., SOWDAMINI, R., RAMAKRISHNA, C. AND BALARAM, P. — *FEBS Lett.*, 1993, **321**, 79–83.
11. DATTA, S. *et al.* — *J. Am. Chem. Soc.*, 1997, **119**, 9246–9251.
12. BARRON, L. D., HECHT, L. AND WILSON, G. — *Biochemistry*, 1997, **36**, 13143–13147.
13. ANET, F. A. L. — *Top. Curr. Chem.*, 1974, **45**, 169–220.
14. KARLE, I. L. AND BALARAM, P. — *Biochemistry*, 1990, **29**, 6747–6756.